

Simple shear in nonlinear Cosserat micropolar elasticity: Existence of minimizers, numerical simulations, and occurrence of microstructure

Mathematics and Mechanics of Solids
2023, Vol. 28(7) 1576–1602

© The Author(s) 2022

Article reuse guidelines:

sagepub.com/journals-permissions

DOI: 10.1177/10812865221122191

journals.sagepub.com/home/mms



Thomas Blesgen 

Bingen University of Applied Sciences, Bingen, Germany

Patrizio Neff

Faculty of Mathematics, University of Duisburg-Essen, Essen, Germany

Received 20 June 2022; accepted 29 July 2022

Abstract

Deformation microstructure is studied for a 1D-shear problem in geometrically nonlinear Cosserat elasticity. Microstructure solutions are described analytically and numerically for zero characteristic length scale.

Keywords

Cosserat theory, microstructure, calculus of variations, micropolar, generalized continuum

1. Introduction

This article studies the formation of microstructure due to simple shear boundary conditions within a geometrically nonlinear Cosserat theory.

The Cosserat model is one of the best-known generalized continuum models [1]. It assumes that material points can undergo translation, described by the standard deformation map $\varphi : \Omega \rightarrow \mathbb{R}^3$ and independent rotations described by the orthogonal tensor field $R : \Omega \rightarrow \text{SO}(3)$, where $\Omega \subset \mathbb{R}^3$ describes the reference configuration of the material. Therefore, the geometrically nonlinear Cosserat model induces immediately the Lie-group structure on the configuration space $\mathbb{R}^3 \times \text{SO}(3)$.

Both fields are coupled in the assumed elastic energy $W = W(\mathbf{D}\varphi, R, \mathbf{D}R)$ and the static Cosserat model appears as a two-field minimization problem which is automatically geometrically nonlinear due to the presence of the non-abelian rotation group $\text{SO}(3)$. Material frame-indifference (objectivity) dictates left-invariance of the Lagrangian W under the action of $\text{SO}(3)$ and material symmetry (here isotropy) implies right-invariance under action of $\text{SO}(3)$.

In the early 20th century, the Cosserat brothers E. and F. Cosserat introduced this model in its full geometrically nonlinear splendor [2] in a bold attempt to unify field theories embracing mechanics,

Corresponding author:

Thomas Blesgen, Bingen University of Applied Sciences, Berlinstraße 109, Bingen D-55411, Germany.

Email: t.blesgen@th-bingen.de

optics and electrodynamics through a common principal of least action. They used the invariance of the energy under Euclidean transformations [3,4] to deduce the correct form of the energy $W = W(R^T \mathbf{D}\varphi, R^T \partial_x R, R^T \partial_y R, R^T \partial_z R)$ and to derive the equations of balance of forces (variations w.r.t. the deformation φ , the force-stress tensor may lose symmetry)[5], and balance of angular momentum (variations w.r.t. rotations R). The Cosserat brothers did not provide, however, any specific constitutive form of the energy since they were not interested in specific applications.

1.1. Three-dimensional geometrically nonlinear isotropic Cosserat model

The underlying three-dimensional isotropic Cosserat model can be described in terms of the standard deformation mapping $\varphi : \Omega \subset \mathbb{R}^3 \rightarrow \mathbb{R}^3$ and an additional orthogonal microrotation tensor $R : \Omega \subset \mathbb{R}^3 \rightarrow \text{SO}(3)$.

The goal here is to find a minimizer of the following isotropic energy (The volumetric term $(\frac{\lambda}{4})((\det \bar{U} - 1)^2 + ((\frac{1}{\det \bar{U}}) - 1)^2)$ is independent of the microrotation R and polyconvex in $\mathbf{D}\varphi$. Its quadratic approximation is $(\frac{\lambda}{2})\text{tr}^2(\bar{U} - \mathbf{1})$.):

$$\begin{aligned}
 E(\varphi, R) &= \int_{\Omega} \mu |\text{sym}(\bar{U} - \mathbf{1}_3)|^2 + \mu_c |\text{skew}(\bar{U} - \mathbf{1}_3)|^2 + \frac{\lambda}{4} \left((\det \bar{U} - 1)^2 + \left(\frac{1}{\det \bar{U}} - 1 \right)^2 \right) \\
 &\quad + \mu \frac{L_c^2}{2} \left(a_1 |\text{dev sym } R^T \text{Curl} R|^2 + a_2 |\text{skew } R^T \text{Curl} R|^2 + \frac{a_3}{3} \text{tr}(R^T \text{Curl} R)^2 \right) dx \tag{1} \\
 &= \int_{\Omega} W_{\text{mp}}(\bar{U}) + W_{\text{disloc}}(R^T \text{Curl} R) dx \rightarrow \min \quad \text{w.r.t. } (\varphi, R), \quad \bar{U} = R^T \mathbf{D}\varphi.
 \end{aligned}$$

The problem will be supplemented by Dirichlet boundary conditions for the deformation φ and the microrotations R can either be left free or prescribed or connected to $\mathbf{D}\varphi$ via the coupling condition $\text{skew}(\bar{U})|_{\Gamma} = 0$ with $\Gamma = \partial\Omega$. Here, $\mu > 0$ is the standard elastic shear modulus, λ the second elastic Lamé parameter, and $\mu_c \geq 0$ is the so-called Cosserat couple modulus; a_1, a_2, a_3 are non-dimensional non-negative weights and $L_c > 0$ is a characteristic length. The isotropic energy (1) is written in terms of the non-symmetric Biot type stretch tensor $\bar{U} = R^T \mathbf{D}\varphi$ (first Cosserat deformation tensor[2]) and the curvature measure $R^T \text{Curl} R$. We call $\alpha := R^T \text{Curl} R$ the *second order* dislocation density tensor [6]. Due to the orthogonality of dev sym, skew and $\text{tr}(\cdot)\mathbf{1}$, the curvature energy provides a complete control of

$$|\alpha|^2 = |R^T \text{Curl} R|^2 = |\text{Curl} R|^2 \quad \text{provided} \quad a_1, a_2, a_3 > 0. \tag{2}$$

Using the result in Neff and Münch [7],

$$|\text{Curl} R|_{\mathbb{R}^{3 \times 3}}^2 \geq c^+ |\mathbf{D}R|_{\mathbb{R}^{3 \times 3 \times 3}}^2, \tag{3}$$

shows that the energy (1) controls $\mathbf{D}R$ in $L^2(\Omega, \mathbb{R}^{3 \times 3 \times 3})$.

In this setting, the minimization problem is highly non-convex w.r.t. (φ, R) . Existence of minimizers for (1) with $\mu_c > 0$ has been shown first in Neff [8] see also [6,8–11], the partial regularity for minimizers of a related problem is investigated in Li and Wang [12] and Gastel [13]. The Cosserat couple modulus μ_c controls the deviation of the microrotation R from the continuum rotation $\text{polar}(\mathbf{D}\varphi)$ in the polar decomposition of $\mathbf{D}\varphi = \text{polar}(\mathbf{D}\varphi) \cdot \sqrt{\mathbf{D}\varphi^T \mathbf{D}\varphi}$, cf. Neff et al. [14].

For $\mu_c \rightarrow \infty$, the constraint $R = \text{polar}(\mathbf{D}\varphi)$ is generated and the model would turn into a Toupin couple stress model.

Here, we derive the three-dimensional Euler–Lagrange equations based on the curvature expressed in the dislocation tensor $\alpha = R^T \text{Curl} R$. We can write the bulk elastic energy as

$$E(\varphi, R) = \int_{\Omega} W_{\text{mp}}(\bar{U}) + W_{\text{disloc}}(\alpha) dx, \quad \bar{U} = R^T \mathbf{D}\varphi, \quad \alpha = R^T \text{Curl} R. \tag{4}$$

Taking variations of Equation (4) w.r.t. the deformation φ leads to

$$\begin{aligned} \delta E(\varphi, R) \cdot \delta \varphi &= \int_{\Omega} \langle \mathbf{D}W_{\text{mp}}(\bar{U}), R^T \mathbf{D}\delta\varphi \rangle_{\mathbb{R}^{3 \times 3}} \, dx = 0, \quad \forall \delta\varphi \in C_0^\infty(\Omega, \mathbb{R}^3) \\ &\Leftrightarrow \int_{\Omega} \langle R \mathbf{D}W_{\text{mp}}(\bar{U}), \mathbf{D}\delta\varphi \rangle_{\mathbb{R}^{3 \times 3}} \, dx = \int_{\Omega} \langle \text{Div}[R \cdot \mathbf{D}W_{\text{mp}}(\bar{U})], \delta\varphi \rangle_{\mathbb{R}^3} \, dx = 0. \end{aligned} \quad (5)$$

Taking variation w.r.t. $R \in \text{SO}(3)$ results in (abbreviate $F := \mathbf{D}\varphi$)

$$\begin{aligned} \delta E(\varphi, R) \cdot \delta R &= \int_{\Omega} \langle \mathbf{D}W_{\text{mp}}(\bar{U}), \delta R^T F \rangle + \langle \mathbf{D}W_{\text{disloc}}(\alpha), \delta R^T \text{Curl}R + R^T \text{Curl}\delta R \rangle \, dx \\ &= \int_{\Omega} \langle \mathbf{D}W_{\text{mp}}(\bar{U}), \delta R^T R \cdot R^T F \rangle + \langle \mathbf{D}W_{\text{disloc}}(\alpha), \delta R^T R \cdot R^T \text{Curl}R + R^T \text{Curl}\delta R \rangle \, dx \\ &= \int_{\Omega} \langle \mathbf{D}W_{\text{mp}}(\bar{U}) \cdot \bar{U}^T, \delta R^T R \rangle + \langle \mathbf{D}W_{\text{disloc}}(\alpha), \delta R^T R \cdot \alpha + R^T \text{Curl}\delta R \rangle \, dx = 0. \end{aligned} \quad (6)$$

Since $R^T R = \mathbf{1}$, it follows that $\delta R^T R + R^T \delta R = 0$ and $\delta R^T R = A \in \mathfrak{so}(3)$ is arbitrary. Therefore, Equation (6) can be written as

$$0 = \int_{\Omega} \langle \mathbf{D}W_{\text{mp}}(\bar{U}) \cdot \bar{U}^T, A \rangle + \langle \mathbf{D}W_{\text{disloc}}(\alpha) \cdot \alpha^T, A \rangle + \langle \mathbf{D}W_{\text{disloc}}(\alpha), R^T \text{Curl}(R A^T) \rangle \, dx \quad (7)$$

for all $A \in C_0^\infty(\Omega, \mathfrak{so}(3))$. Using that Curl is a self-adjoint operator, this is equal to

$$\begin{aligned} 0 &= \int_{\Omega} \langle \mathbf{D}W_{\text{mp}}(\bar{U}) \cdot \bar{U}^T + \mathbf{D}W_{\text{disloc}}(\alpha) \alpha^T, A \rangle + \langle \text{Curl}(R \mathbf{D}W_{\text{disloc}}(\alpha)), R A^T \rangle \, dx \\ &= \int_{\Omega} \langle \mathbf{D}W_{\text{mp}}(\bar{U}) \cdot \bar{U} + \mathbf{D}W_{\text{disloc}}(\alpha) \alpha^T - R^T \text{Curl}(R \mathbf{D}W_{\text{disloc}}(\alpha)), A \rangle \, dx \quad \forall A \in C_0^\infty(\Omega, \mathfrak{so}(3)). \end{aligned} \quad (8)$$

Thus, the strong form of the Euler–Lagrange equations reads

$$\begin{aligned} \text{Div}[R \mathbf{D}W_{\text{mp}}(\bar{U})] &= 0, && \text{"balance of forces"}, \\ \text{skew}[R^T \text{Curl}(R \mathbf{D}W_{\text{disloc}}(\alpha))] &= \text{skew}(\mathbf{D}W_{\text{mp}}(\bar{U}) \cdot \bar{U}^T + \mathbf{D}W_{\text{disloc}}(\alpha) \cdot \alpha^T), && \text{"balance of angular momentum"} \end{aligned} \quad (9)$$

If $\mathbf{D}W_{\text{disloc}}(\alpha) \equiv 0$ (no moment stresses, zero characteristic length $L_c = 0$), then balance of angular momentum turns into the symmetry constraint

$$\mathbf{D}W_{\text{mp}}(\bar{U}) \cdot \bar{U}^T \in \text{Sym}(3). \quad (10)$$

A complete discussion of the solutions [15] to this constraint and applications can be found in Neff and others [4,16–18].

2. The Cosserat model in simple shear

To elucidate the proposed nonlinear theory, notably the impact of boundary and side conditions on the microrotations, cf. figure 1, we consider the deformation of an infinite layer of material with unit height, fixed at the bottom and sheared in e_1 -direction with amount γ at the upper face. We impose the boundary conditions $\varphi(x_1, x_2, 0) = (x_1, x_2, 0)^T$, $\varphi(x_1, x_2, 1) = (x_1 + \gamma, x_2, x_3)^T$, $x_1, x_2 \in \mathbb{R}$. The parameter $\gamma \geq 0$ is the amount of maximal shear at the upper face per unit length. The most general deformations are of the form

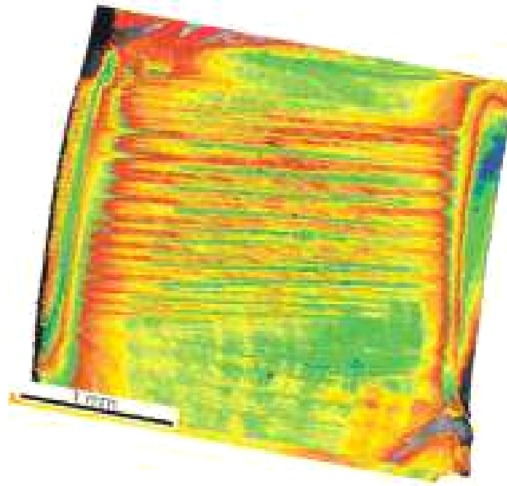


Figure 1. A single crystal copper specimen in simple shear, showing glide planes and micro bands. Lattice rotations do not coincide with continuum rotations. Courtesy of D. Raabe, MPI-Eisenforschung, Düsseldorf [19].

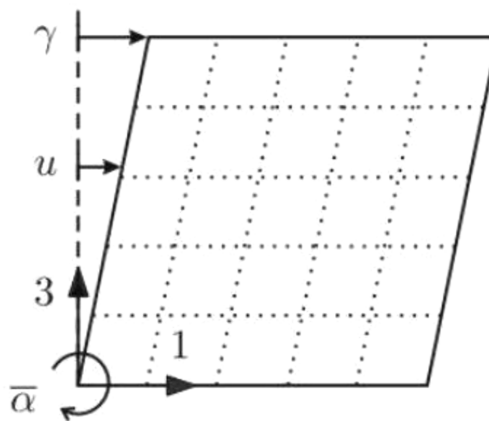


Figure 2. The deformed state exhibits a homogeneous region in the interior of the structure which motivates the kinematics of simple shear.

$$\varphi(x_1, x_2, x_3) = (x_1 + u(x_1, x_2), x_2, x_3 + v(x_1, x_3))^T,$$

see Figure 2. Hence, we look for energy minimizing deformations in the form

$$\varphi(x_1, x_2, x_3) = \begin{pmatrix} x_1 + u(x_1, x_3) \\ x_2 \\ x_3 + v(x_1, x_3) \end{pmatrix}, \quad D\varphi(x_1, x_2, x_3) = \begin{pmatrix} 1 + u_{x_1}(x_1, x_3) & 0 & u_{x_3}(x_1, x_3) \\ 0 & 1 & 0 \\ v_{x_1}(x_1, x_3) & 0 & 1 + v_{x_3}(x_1, x_3) \end{pmatrix}, \quad (11)$$

with $u(x_1, 0) = 0, u(x_1, 1) = \gamma$. The infinite extension in e_1 -direction implies that ∂_{x_1} must vanish and from symmetry of the boundary conditions at the upper and lower face, there is no reason for a displacement in e_3 -direction either. Hence, the reduced kinematics

$$\varphi(x_1, x_2, x_3) = \begin{pmatrix} x_1 + u(x_3) \\ x_2 \\ x_3 \end{pmatrix}, \quad F = D\varphi(x_1, x_2, x_3) = \begin{pmatrix} 1 & 0 & u'(x_3) \\ 0 & 1 & 0 \\ 0 & 0 & 1 \end{pmatrix}, \quad (12)$$

with $u(0) = 0$, $u(1) = \gamma$ suffices. The considered problem is therefore the exact formulation of the simple shear in e_1 -direction with amount γ at the upper face of a layer of material with unit height, fixed at the bottom.

Accordingly, we assume microrotations $R \in \text{SO}(3)$ in the form

$$R(x_1, x_2, x_3) = \begin{pmatrix} \cos \alpha(x_3) & 0 & \sin \alpha(x_3) \\ 0 & 1 & 0 \\ -\sin \alpha(x_3) & 0 & \cos \alpha(x_3) \end{pmatrix}, \quad (13)$$

having fixed axis of rotation e_2 . Therefore,

$$\text{Curl}R = \begin{pmatrix} 0 & -\sin \alpha(x_3)\alpha'(x_3) & 0 \\ 0 & 0 & 0 \\ 0 & -\cos \alpha(x_3)\alpha'(x_3) & 0 \end{pmatrix}. \quad (14)$$

In the following, we denote x_3 by x . It holds $|\bar{R}^T \text{Curl}\bar{R}|^2 = |\text{Curl}\bar{R}|^2 = |\bar{\alpha}'|^2$.

Inserting the ansatz (11) and (13) leaves us with the energy

$$\begin{aligned} E(u, \alpha) &= \int_0^1 W(u', \alpha, \alpha') \, dx \\ &:= \mu \int_0^1 2L_c^2 |\alpha'|^2 + 2(\cos(\alpha) - 1)^2 + \frac{1 + \sin^2(\alpha)}{2} |u'|^2 + 2(\cos(\alpha) - 1) \sin(\alpha) u' \, dx \\ &\quad + \frac{\mu_c}{2} \int_0^1 \cos^2(\alpha) (2 \tan(\alpha) - u')^2 \, dx. \end{aligned} \quad (15)$$

3. A one-dimensional simple shear problem

In this article, we are now concerned with minimizers of the *mechanical energy functional*

$$\begin{aligned} E(u, \alpha) &= \mu \int_0^1 2L_c^2 |\alpha'|^2 + 2(\cos(\alpha) - 1)^2 + \frac{1 + \sin^2(\alpha)}{2} |u'|^2 + 2(\cos(\alpha) - 1) \sin(\alpha) u' \, dx \\ &\quad + \frac{\mu_c}{2} \int_0^1 \cos^2(\alpha) (2 \tan(\alpha) - u')^2 \, dx. \end{aligned} \quad (16)$$

Introducing the third-order expansion $\cos(\alpha) \sim 1 - (\frac{\alpha^2}{2})$, $\sin(\alpha) \sim \alpha - (\frac{\alpha^3}{6})$ and dropping the higher order terms leads to the *reduced mechanical energy functional*

$$\begin{aligned} E_{\text{red}}(u, \alpha) &:= \mu \int_0^1 \left(2L_c^2 |\alpha'|^2 + \frac{1 + \alpha^2}{2} |u'|^2 + \frac{\alpha^4}{2} - \alpha^3 u' \right) dx \\ &\quad + 2\mu_c \int_0^1 \left(\frac{u'}{2} - \alpha \right) \left(\frac{u'}{2} - \alpha - \frac{\alpha^2}{6} (3u' - 2\alpha) \right) dx. \end{aligned} \quad (17)$$

For the definitions (16) and (17), see also [20][Equation (3.11), Equation (3.22)]. We first provide alternative representations of these two functionals as this allows to simplify the Euler–Lagrange equations and will give insights into the minimizers later.

Lemma 1. The functionals E , E_{red} defined in Equations (16) and (17) can alternatively be written as

$$E(u, \alpha) = \int_0^1 W(u', \alpha, \alpha') \, dx \quad (18)$$

$$\begin{aligned}
 &= \frac{\mu}{2} \int_0^1 4L_c^2 |\alpha'|^2 + |u'|^2 + \left(\sin(\alpha)u' - 4 \sin^2\left(\frac{\alpha}{2}\right) \right)^2 dx \\
 &\quad + \frac{\mu_c}{2} \int_0^1 (\cos(\alpha)u' - 2 \sin(\alpha))^2 dx,
 \end{aligned} \tag{19}$$

$$\begin{aligned}
 E_{\text{red}}(u, \alpha) &= \frac{\mu}{2} \int_0^1 4L_c^2 |\alpha'|^2 + |u'|^2 + [\alpha(\alpha - u')]^2 dx \\
 &\quad + \frac{\mu_c}{2} \int_0^1 (1 - \alpha^2)|u'|^2 + \left(\frac{8\alpha^2}{3} - 4\right)\alpha u' + 4\alpha^2 - \frac{4\alpha^4}{3} dx.
 \end{aligned} \tag{20}$$

Proof. Both identities follow from straightforward elementary rearrangements. Trigonometric addition formulas imply $\cos(2\alpha) = \cos^2(\alpha) - \sin^2(\alpha) = 1 - 2 \sin^2(\alpha)$; hence,

$$\cos(\alpha) - 1 = -2 \sin^2\left(\frac{\alpha}{2}\right). \tag{21}$$

Plugging Equation (21) into Equation (16) yields

$$\begin{aligned}
 &2(\cos(\alpha) - 1)^2 + \frac{1 + \sin^2(\alpha)}{2} |u'|^2 + 2(\cos(\alpha) - 1) \sin(\alpha) u' \\
 &= 8 \sin^4\left(\frac{\alpha}{2}\right) + \frac{|u'|^2}{2} + \frac{\sin^2(\alpha)|u'|^2}{2} - 4u' \sin^2\left(\frac{\alpha}{2}\right) \sin(\alpha) \\
 &= \frac{1}{2} \left(\sin(\alpha)u' - 4 \sin^2\left(\frac{\alpha}{2}\right) \right)^2 + \frac{|u'|^2}{2}.
 \end{aligned} \tag{22}$$

Similarly, for the μ_c -integral in Equation (16),

$$\begin{aligned}
 \cos^2(\alpha)(2 \tan(\alpha) - u')^2 &= \cos^2(\alpha)(4 \tan^2(\alpha) - 4 \tan(\alpha)u' + |u'|^2) \\
 &= 4 \sin^2(\alpha) - 4 \sin(\alpha) \cos(\alpha)u' + \cos^2(\alpha)|u'|^2 = (\cos(\alpha)u' - 2 \sin(\alpha))^2.
 \end{aligned} \tag{23}$$

This proves Equation (19). The proof of Equation (20) is immediate from

$$\frac{1 + \alpha^2}{2} |u'|^2 + \frac{\alpha^4}{2} - \alpha^3 u' = \frac{|u'|^2}{2} + \frac{\alpha^2}{2} (|u'|^2 - 2\alpha u' + \alpha^2),$$

and a re-ordering of the μ_c -integral.

Remark 1. The μ_c -part of E_{red} cannot be written as a complete quadratic form since some higher order terms have been dropped. However, by keeping the terms $\frac{\mu_c}{2} \left(\frac{\alpha^4}{4} |u'|^2 - \frac{1}{3} \alpha^5 u' + \frac{1}{9} \alpha^6 \right)$ of the Taylor expansion of W , we find

$$E_{\text{red}}(u, \alpha) = \int_0^1 W_{\text{red}}(u', \alpha, \alpha') dx \tag{24}$$

$$= \frac{\mu}{2} \int_0^1 4L_c^2 |\alpha'|^2 + |u'|^2 + [\alpha(\alpha - u')]^2 dx + \frac{\mu_c}{2} \int_0^1 \left(\frac{2 - \alpha^2}{2} u' - \frac{6\alpha - \alpha^3}{3} \right)^2 dx. \tag{25}$$

From now on we will use this representation (25) instead of (20).

We consider the minimization problem

$$E(u, \alpha) \rightarrow \min \tag{26}$$

subject either to the *consistent coupling conditions* [21] (derived from $\text{skew}(R^T F)|_{\{0,1\}} = 0$)

$$u(0) = 0, \quad u(1) = \gamma, \quad u'(0) = 2 \tan(\alpha(0)), \quad u'(1) = 2 \tan(\alpha(1)) \quad (27)$$

or subject to the *Dirichlet boundary conditions* (for prescribed microrotation angle $\alpha_D \in \mathbb{R}$ at the upper and lower faces)

$$u(0) = 0, \quad u(1) = \gamma, \quad \alpha(0) = \alpha(1) = \alpha_D. \quad (28)$$

To single out solutions, we may impose the further *symmetry constraint*

$$u'(1) = u'(0). \quad (29)$$

The Euler–Lagrange equations related to Equation (26), replacing [20][Equation (3.14)], read

$$[2\mu + (\mu_c - \mu) \cos^2(\alpha)]u'' = 2(\mu_c - \mu)(\sin(\alpha) \cos(\alpha)u' + \cos^2(\alpha) - \sin^2(\alpha))\alpha' + 2\mu \cos(\alpha)\alpha', \quad (30)$$

$$4\mu L_c^2 \alpha'' = (\cos(\alpha)u' - 2 \sin(\alpha)) \left[(\mu - \mu_c) \left(\sin(\alpha)u' - 4 \sin^2\left(\frac{\alpha}{2}\right) \right) - 2\mu_c \right] \quad (31)$$

for $x = x_3 \in \Omega := (0, 1)$ subject to either Equations (27), (29) or (28), (29). The Equations (30) and (31) constitute balance of force and angular momentum, respectively. Equation (31) is the form that Equation (10) takes for the ansatz made here.

Equation (30) is equivalent to $(d/dx)\tau(u, \alpha) = 0$ in Ω for the *force stress tensor* $\tau = \tau(u, \alpha)$ defined by

$$\tau := D_{u'} W(u', \alpha, \alpha') = \mu \left[u' + \sin(\alpha) \left(\sin(\alpha)u' - 4 \sin^2\left(\frac{\alpha}{2}\right) \right) \right] + \mu_c \cos(\alpha) [\cos(\alpha)u' - 2 \sin(\alpha)]. \quad (32)$$

The Euler–Lagrange equations related to $E_{\text{red}}(u, \alpha) \rightarrow \min$ lead to the *reduced system*

$$\begin{aligned} - \left[\mu(1 + \alpha^2) + \mu_c \left(1 - \alpha^2 + \frac{1}{4}\alpha^4 \right) \right] u'' &= (4\mu_c - 3\mu)\alpha^2 \alpha' + 2(\mu - \mu_c)\alpha \alpha' u' - 2\mu_c \alpha' \\ &\quad + \mu_c \alpha^3 \left(u' - \frac{5}{6}\alpha \right) \alpha', \end{aligned} \quad (33)$$

$$\begin{aligned} \mu \left(-L_c^2 \alpha'' + \frac{1}{2}\alpha^3 - \frac{3}{4}\alpha^2 u' + \frac{1}{4}\alpha |u'|^2 \right) + \mu_c \left(-\frac{1}{4}\alpha |u'|^2 + \alpha^2 u' - \frac{2}{3}\alpha^3 + \alpha - \frac{1}{2}u' \right) \\ + \mu_c \left(\frac{1}{8}\alpha^3 |u'|^2 - \frac{5}{24}\alpha^4 u' + \frac{1}{12}\alpha^5 \right) = 0 \end{aligned} \quad (34)$$

for $x = x_3 \in \Omega := (0, 1)$ subject either to the reduced consistent coupling boundary conditions

$$u(0) = 0, \quad u(1) = \gamma, \quad 2\alpha(0) = u'(0), \quad 2\alpha(1) = u'(1) \quad (35)$$

and Equation (29) or subject to Equations (28) and (29). Underlined in Equations (33) and (34) are those higher order terms that are only present if E_{red} is defined by Equation (25) instead of Equation (17) or (20).

Equation (33) is equivalent to $(d/dx)\tau_{\text{red}}(u, \alpha) = 0$ in Ω for the *reduced force stress tensor* $\tau_{\text{red}} = \tau_{\text{red}}(u, \alpha)$ defined by

$$\tau_{\text{red}} := D_{u'} W(u', \alpha, \alpha') = \mu [u' - \alpha^2(\alpha - u')] + \mu_c \left(\frac{2 - \alpha^2}{2} \right) \left[\frac{2 - \alpha^2}{2} u' - \frac{6\alpha - \alpha^3}{3} \right]. \quad (36)$$

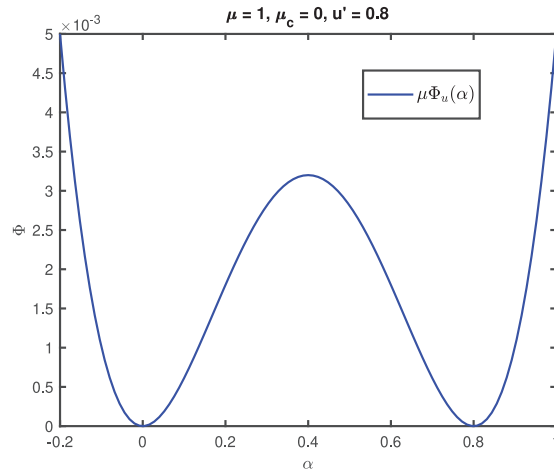


Figure 3. The double-well potential $\mu\Phi_u(\alpha)$ for $\alpha \in [-0.2, 1]$, $u' = 0.8$ and $\mu = 1$.

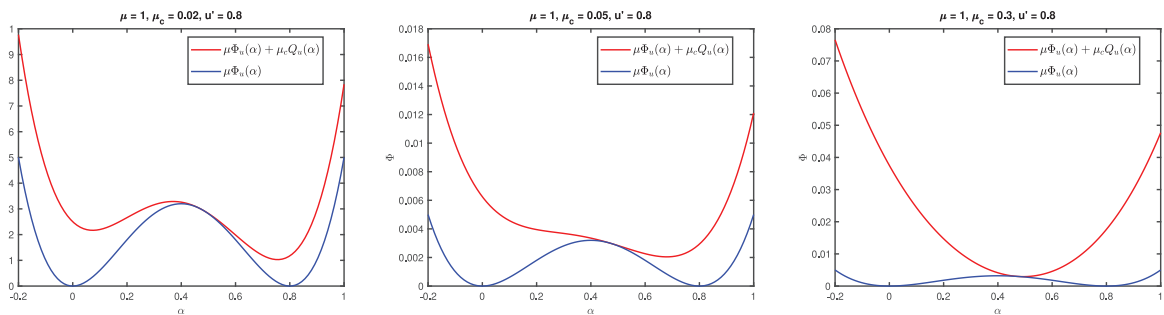


Figure 4. The potential $\mu\Phi_u(\alpha) + \mu_c Q_u(\alpha)$ (in red) compared with the double-well potential $\mu\Phi_u(\alpha)$ (in blue) for $\alpha \in [-0.2, 1]$, $u' = 0.8$ and $\mu = 1$. Left: $\mu_c = 0.02$. Center: $\mu_c = 0.05$. Right: $\mu_c = 0.3$.

We point out that Equation (34) can equally be written as

$$\mu L_c^2 \alpha'' = \mu \partial_\alpha \Phi_u(\alpha) + \mu_c \partial_\alpha Q_u(\alpha) \tag{37}$$

with the potentials

$$\Phi_u(\alpha) := \frac{1}{8} \alpha^2 (\alpha - u')^2, \quad Q_u(\alpha) := \frac{1}{8} \left(\frac{2 - \alpha^2}{2} u' - \frac{6\alpha - \alpha^3}{3} \right)^2. \tag{38}$$

For small values $\mu_c \geq 0$, the double-well potential Φ_u (see Figure 3) is dominant and Equation (37) corresponds to a stationary Allen–Cahn equation (Allen–Cahn equation: $\partial_t u = \varepsilon \Delta u - \psi'(u)$ with a double-well potential ψ). The larger the Cosserat couple modulus μ_c , the stronger the influence of the quadratic potential Q_u . There is a bifurcation and a critical value μ_c^{crit} , such that for $\mu_c \geq \mu_c^{crit}$, the right-hand side of Equation (37) has only one minimizer (see Figure 4).

Related to different boundary conditions, we introduce the reflexive Banach spaces

$$\begin{aligned} \mathcal{X}^D &:= \left\{ (u, \alpha) \in (W^{1,2}(\Omega; \mathbb{R}))^2 \mid u(0) = 0, u(1) = \gamma, \alpha(0) = \alpha(1) = \alpha_D \right\}, \\ \mathcal{X}^D &:= \left\{ (u, \alpha) \in W^{1,2}(\Omega; \mathbb{R}) \times L^4(\Omega; \mathbb{R}) \mid u(0) = 0, u(1) = \gamma, \alpha(0) = \alpha(1) = \alpha_D \right\} \end{aligned} \tag{39}$$

and correspondingly for the consistent coupling conditions

$$\begin{aligned}
\mathcal{X}_{\text{red}}^C &:= \left\{ (u, \alpha) \in (W^{1,2}(\Omega; \mathbb{R}))^2 \mid u(0) = 0, u(1) = \gamma, 2\alpha(0) = u'(0), 2\alpha(1) = u'(1) \right\}, \\
\mathcal{X}^C &:= \left\{ (u, \alpha) \in (W^{1,2}(\Omega; \mathbb{R}))^2 \mid u(0) = 0, u(1) = \gamma, 2 \tan \alpha(0) = u'(0), 2 \tan \alpha(1) = u'(1) \right\}, \\
X_{\text{red}}^C &:= \left\{ (u, \alpha) \in W^{1,2}(\Omega; \mathbb{R}) \times L^4(\Omega; \mathbb{R}) \mid u(0) = 0, u(1) = \gamma, 2\alpha(0) = u'(0), 2\alpha(1) = u'(1) \right\}, \\
X^C &:= \left\{ (u, \alpha) \in W^{1,2}(\Omega; \mathbb{R}) \times L^4(\Omega; \mathbb{R}) \mid u(0) = 0, u(1) = \gamma, 2 \tan \alpha(0) = u'(0), 2 \tan \alpha(1) = u'(1) \right\}.
\end{aligned} \tag{40}$$

Lemma 2 Let $L_c > 0$. Then, for any $\mu > 0$, $\mu_c \geq 0$, E_{red} defined by Equation (25) possesses a minimizer (u, α) in $\mathcal{X}_{\text{red}}^C$, \mathcal{X}^D and E possesses a minimizer in \mathcal{X}^C , \mathcal{X}^D . For $L_c = 0$, E_{red} has minimizers in X_{red}^C , X^D and E has minimizers in X^C , X^D .

Proof. (i) Let $L_c > 0$. We first consider the case of Dirichlet boundary conditions for u and α . Rewriting Equation (25) as a functional defined on $\mathcal{X}_0 := (W_0^{1,2}((0, 1); \mathbb{R}))^2$, we find with Young's inequality for $(u, \alpha) \in \mathcal{X}_0$

$$\begin{aligned}
E_{\text{red}}(u + \gamma, \alpha + \alpha_D) &= \frac{\mu}{2} \int_0^1 4L_c^2 |\alpha'|^2 + (u' + \gamma)^2 + [(\alpha + \alpha_D)(\alpha + \alpha_D - (u' + \gamma))]^2 dx \\
&\quad + \frac{\mu_c}{2} \int_0^1 \left(\frac{2 - (\alpha + \alpha_D)^2}{2} (u' + \gamma) - \frac{6(\alpha + \alpha_D) - (\alpha + \alpha_D)^3}{3} \right)^2 dx \\
&\geq \frac{\mu}{2} \int_0^1 4L_c^2 |\alpha'|^2 + (u' + \gamma)^2 dx \\
&= \mu \int_0^1 2L_c^2 |\alpha'|^2 + \frac{1}{2} |u'|^2 + \left(\frac{u'}{2} \right) (2\gamma) + \frac{\gamma^2}{2} dx \\
&\geq \mu \int_0^1 2L_c^2 |\alpha'|^2 + \frac{1}{2} |u'|^2 - \frac{1}{4} |u'|^2 - 4\gamma^2 + \frac{\gamma^2}{2} dx \\
&= \mu \int_0^1 2L_c |\alpha'|^2 + \frac{1}{4} |u'|^2 - \frac{7\gamma^2}{2} dx.
\end{aligned} \tag{41}$$

With the Poincaré inequality valid on \mathcal{X}_0 and the Banach–Alaoglu theorem, this demonstrates that the level sets

$$\{(u, \alpha) \in \mathcal{X}^D \mid E_{\text{red}}(u, \alpha) \leq C\}$$

for constants $C > 0$ are sequentially weakly precompact proving the coercivity of E_{red} , see, for example, Struwe [22].

We observe that the integrand $W_{\text{red}}(u', \alpha, \alpha')$ as defined in Equation (24) is a Carathéodory function and strictly convex both in u' and α' . Despite the dependence of W_{red} on α , the proof of weak lower semicontinuity of E_{red} in \mathcal{X}^D can thus be carried out in the spirit of the well-known Tonelli–Serrin theorem, see Dacorogna [23, Section 3.2.6] for details. Alternatively, the weak lower semicontinuity can be derived from the more general result in Acerbi and Fusco [24] based on gradient Young measures. By the direct method in the calculus of variations, the coercivity and weak lower semicontinuity of E_{red} yield the existence of a minimizer $(u, \alpha) \in \mathcal{X}^D$. The proof of minimizers of E_{red} in $\mathcal{X}_{\text{red}}^C$ is similar.

Now let us consider the case of Dirichlet boundary conditions for E . Proceeding as above and estimating the quadratic terms from below by 0, we find for $(u, \alpha) \in \mathcal{X}_0$

$$E(u + \gamma, \alpha + \alpha_D) \geq \frac{\mu}{2} \int_0^1 4L_c^2 |\alpha'|^2 + (u' + \gamma)^2 dx.$$

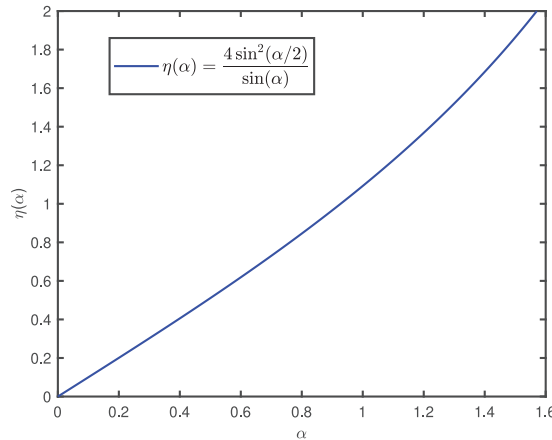


Figure 5. Plot of the function $\eta(\alpha) = \frac{4 \sin^2(\frac{\alpha}{2})}{\sin(\alpha)}$ for $\alpha \in [0, \frac{\pi}{2}]$.

This coincides with Equation (41). From there, with the Poincaré inequality the coercivity of E in \mathcal{X}^D can be shown as above. The lower semicontinuity of E is again a consequence of strict convexity and the Tonelli–Serrin theorem. The proof of minimizers of E in \mathcal{X}^C is similar.

- ii. Let $L_c = 0$. The coercivity of E_{red} w.r.t. weak-convergence can be shown similar to (i). In contrast, E is 2π -periodic in α which replaces the coercivity in α . Equations (25) and (19) imply the lower semicontinuity of E_{red} and E . With the direct method, the existence of minimizers of E_{red} in \mathcal{X}^D , \mathcal{X}^C and of E in \mathcal{X}^D , \mathcal{X}^C for any $\mu > 0$, $\mu_c \geq 0$ follows. \square

For the detailed discussion of the Euler–Lagrange equations related to problem (26), we introduce the function

$$\eta(\alpha) := \frac{4 \sin^2(\frac{\alpha}{2})}{\sin(\alpha)}. \tag{42}$$

It holds $\lim_{\alpha \rightarrow 0} \eta(\alpha) = 0$ and $\eta(\alpha)$ is invertible, monotone increasing and close to a linear function (cf. Figure 5).

In the following discussion, we first ignore the boundary conditions on u and α and study sufficiently regular solutions $u \in W^{2,2}(\Omega)$ and $\alpha \in W^{1,2}(\Omega)$. Clearly, not every solution is in this class (cf. Section 4).

Lemma 3. Let $L_c = 0$ and $\mu > 0$, $\mu_c \geq 0$. Then every solution

$$(u, \alpha) \in W^{2,2}(\Omega) \times W^{1,2}(\Omega)$$

of the Euler–Lagrange Equations (30) and (31) is continuous in $\overline{\Omega}$ and satisfies

$$u''(x) = \alpha'(x) = 0 \text{ for a.e. } x \in \Omega. \tag{43}$$

Proof. Due to the Sobolev embedding $W^{1,2}(\Omega) \hookrightarrow C^0(\overline{\Omega})$, both α and u are continuous.

- i. For $\mu = \mu_c$, the Euler–Lagrange Equations (30) and (31) simplify to

$$u'' = \cos(\alpha)\alpha', \tag{44}$$

$$0 = \cos(\alpha)u' - 2 \sin(\alpha) \tag{45}$$

to be satisfied pointwise for $x \in \Omega$.

Equation (45) is equivalent to $u' = 2 \tan(\alpha)$ and taking the derivative yields $u'' = \frac{2\alpha'}{\cos^2(\alpha)}$. With Equation (44), we find

$$\frac{2\alpha'}{\cos^2(\alpha)} = \cos(\alpha)\alpha'. \quad (46)$$

Since $2 = \cos^3(\alpha)$ has no solution, Equation (46) implies $\alpha' = 0$, and so with Equation (44) $u'' = 0$.

ii. Let $\mu > 0$, $\mu_c \geq 0$ with $\mu \neq \mu_c$. Considering the Euler–Lagrange Equation (31) with $L_c = 0$, two cases may occur.

Case 1: $\alpha = \arctan(u'/2)$.

This implies $u' = 2 \tan(\alpha)$ such that $u'' = \frac{2\alpha'}{\cos^2(\alpha)}$. Inserting this identity in Equation (30) yields

$$(\mu_c - \mu) \frac{[\sin(\alpha) \cos(\alpha)u' + \cos^2(\alpha) - \sin^2(\alpha)]\alpha'}{2\mu + (\mu_c - \mu) \cos^2(\alpha)} + \frac{\mu \cos(\alpha)\alpha'}{2\mu + (\mu_c - \mu) \cos^2(\alpha)} = \frac{\alpha'}{\cos^2(\alpha)}. \quad (47)$$

(The denominator in Equation (47) is positive, for example, $2\mu + (\mu_c - \mu) \cos^2(\alpha) \geq 2\mu > 0$ for $\mu_c \geq \mu$ and $2\mu + (\mu_c - \mu) \cos^2(\alpha) \geq 2\mu - (\mu_c - \mu) > 0$ for $\mu_c < \mu$.)

Using $u' = 2 \tan(\alpha)$ on the right gives after simplifications

$$\frac{[\mu_c - \mu + \mu \cos(\alpha)]\alpha'}{2\mu + (\mu_c - \mu) \cos^2(\alpha)} = \frac{\alpha'}{\cos^2(\alpha)} \quad (48)$$

which is equivalent to

$$\mu \cos^3(\alpha)\alpha' = 2\mu\alpha'.$$

Since $\mu > 0$, this proves as in (i) that $\alpha' = 0$ which with Equation (30) results in $u'' = 0$.

Case 2: $\sin(\alpha)u' = 4 \sin^2(\frac{\alpha}{2}) + \frac{2\mu_c}{\mu - \mu_c}$.

For $\mu_c = 0$, one solution is $\alpha \equiv 2\pi k$ for some $k \in \mathbb{Z}$. Then $\alpha' = 0$ and Equation (30) shows $u'' = 0$. Alternatively, for $\alpha \not\equiv 2\pi k$, we have $\sin(\alpha) \neq 0$ such that

$$u' = \frac{2\mu_c}{(\mu - \mu_c) \sin(\alpha)} + \frac{4 \sin^2(\frac{\alpha}{2})}{\sin(\alpha)}. \quad (49)$$

Taking the derivative yields

$$u'' = -\frac{2\mu_c \cos(\alpha)\alpha'}{(\mu - \mu_c) \sin^2(\alpha)} + \frac{[4 \sin(\frac{\alpha}{2}) \cos(\frac{\alpha}{2}) \sin(\alpha) - 4 \sin^2(\frac{\alpha}{2}) \cos(\alpha)]\alpha'}{\sin^2(\alpha)}.$$

We use $4 \sin(\frac{\alpha}{2}) \cos(\frac{\alpha}{2}) = 2 \sin(\alpha)$ and $-4 \sin^2(\frac{\alpha}{2}) = -2 + 2 \cos(\alpha)$. With the Euler–Lagrange equation (30), this leads to

$$\begin{aligned} & -\frac{2\mu_c \cos(\alpha)\alpha'}{(\mu - \mu_c) \sin^2(\alpha)} + \frac{2[\sin^2(\alpha) - \cos(\alpha) + \cos^2(\alpha)]\alpha'}{\sin^2(\alpha)} \\ & = \frac{[2(\mu_c - \mu)(\sin(\alpha) \cos(\alpha)u' + \cos^2(\alpha) - \sin^2(\alpha)) + 2\mu \cos(\alpha)]\alpha'}{2\mu + (\mu_c - \mu) \cos^2(\alpha)} \end{aligned}$$

and simplifies to

$$\begin{aligned} & \frac{\mu_c \cos(\alpha) \alpha'}{(\mu_c - \mu)(1 - \cos^2(\alpha))} + \frac{[1 - \cos(\alpha)] \alpha'}{1 - \cos^2(\alpha)} \\ &= \frac{[(\mu_c - \mu)(\sin(\alpha) \cos(\alpha) u' + \cos^2(\alpha) - \sin^2(\alpha)) + \mu \cos(\alpha)] \alpha'}{2\mu + (\mu_c - \mu) \cos^2(\alpha)}. \end{aligned}$$

On the right, we plug in the expression (49) for u' . So we obtain,

$$\begin{aligned} & \frac{[(\mu_c - \mu)(1 - \cos(\alpha)) + \mu_c \cos(\alpha)] \alpha'}{(\mu_c - \mu)(1 - \cos^2(\alpha))} \\ &= \frac{[-2\mu_c \cos(\alpha) + \mu \cos(\alpha) + (\mu_c - \mu)(2 \cos(\alpha) - 2 \cos^2(\alpha) + \cos^2(\alpha) - \sin^2(\alpha))] \alpha'}{2\mu + (\mu_c - \mu) \cos^2(\alpha)}. \end{aligned}$$

After simplifications, this is equivalent to

$$\frac{[(\mu_c - \mu) + \mu \cos(\alpha)] \alpha'}{(\mu_c - \mu)(1 - \cos^2(\alpha))} = \frac{[-\mu \cos(\alpha) - (\mu_c - \mu)] \alpha'}{2\mu + (\mu_c - \mu) \cos^2(\alpha)}. \tag{50}$$

Expanding this, we find

$$\begin{aligned} & [2\mu(\mu_c - \mu) + 2\mu^2 \cos(\alpha) + (\mu_c - \mu)^2 \cos^2(\alpha) + \mu(\mu_c - \mu) \cos^3(\alpha)] \alpha' \\ &= [-\mu(\mu_c - \mu) \cos(\alpha) - (\mu_c - \mu)^2 + \mu(\mu_c - \mu) \cos^3(\alpha) + (\mu_c - \mu)^2 \cos^2(\alpha)] \alpha'. \end{aligned} \tag{51}$$

This simplifies further to

$$[2\mu^2 + \mu(\mu_c - \mu)] \cos(\alpha) \alpha' = [2\mu(\mu - \mu_c) - (\mu_c - \mu)^2] \alpha' \tag{52}$$

and eventually

$$\mu(\mu + \mu_c) \cos(\alpha) \alpha' = (\mu + \mu_c)(\mu - \mu_c) \alpha'.$$

Hence, either $\alpha' = 0$ or

$$\alpha \equiv \alpha_4 := \arccos\left(\frac{\mu - \mu_c}{\mu}\right) \tag{53}$$

provided $|\frac{\mu - \mu_c}{\mu}| \leq 1$. In both cases, we have $\alpha' = 0$ which shows with (30) that $u'' = 0$. □

Remark 2. The consistent coupling condition is made such that the homogeneous deformation $\bar{u}(x) = \gamma x$ remains a solution of the boundary value problem.

For given $\gamma > 0$ and fixed $k \in \mathbb{Z}$, we introduce the constants

$$\alpha_1 := 2k\pi, \quad \alpha_2 := \arctan\left(\frac{\gamma}{2}\right), \quad \alpha_3 := \eta^{-1}(\gamma).$$

Corollary 1. Any solution $u \in X := \{W^{2,2}(\Omega) \mid u(0) = 0, u(1) = \gamma\}$ to (26) is monotonically increasing. The homogeneous function $\bar{u}(x) := \gamma x$ solves the Euler–Lagrange Equations (30) and (31). Depending on the values of μ and μ_c , the corresponding solution α to Equations (30) and (31) is given by

$$\begin{aligned} (i) \quad \mu = \mu_c : \quad & \alpha(x) \equiv \alpha_2. \\ & (\bar{u}, \alpha_2) \text{ is a local minimizer of } E. \end{aligned} \tag{54}$$

$$(ii) \mu_c = 0 : \quad \alpha(x) \equiv \alpha_1, \alpha(x) \equiv \alpha_2, \alpha(x) \equiv \alpha_3. \quad (55)$$

(\bar{u}, α_1) and (\bar{u}, α_3) are local minimizers of E .

$$(iii) \mu_c > 0, \mu \neq \mu_c : \quad \alpha(x) \equiv \alpha_2. \text{ If} \quad (56)$$

$$2\mu + (\mu_c - \mu)\sqrt{\gamma^2 + 4} > 0, \quad (57)$$

then (\bar{u}, α_2) is a local minimizer of E .

Proof. Due to Lemma 3, any minimizer $u \in W^{2,2}(\Omega)$ to Equation (26) must be piecewise linear. Choosing a function u with $u(0) = 0$, $u(1) = \gamma$ which is not monotonically increasing enlarges the component $(\frac{\mu}{2})|u'|^2$ in W (cf. Equation (19)). With Equation (43), this demonstrates the optimality of $\bar{u}(x)$ in the class X of regular solutions. It remains to find the optimal values of α , and the strict positivity of the second variation $D_\alpha^2(\bar{u}, \alpha)$ is sufficient for that, see (66) below.

For fixed $u \in X$ and a test function $\delta\alpha \in C^\infty((0, 1); \mathbb{R})$, the second variation of E with respect to α is

$$D_\alpha^2 E(u, \alpha)(\delta\alpha, \delta\alpha) = \int_0^1 \left(W_{\alpha\alpha}(u', \alpha, \alpha') - \frac{d}{dx} W_{\alpha\alpha'}(u', \alpha, \alpha') \right) \delta\alpha(x)^2 + W_{\alpha'\alpha'}(u', \alpha, \alpha') \delta\alpha'(x)^2 dx \quad (58)$$

where subscripts denote partial derivatives. Here, we have (cf. Equation (19)),

$$W(u', \alpha, \alpha') = \frac{\mu}{2}|u'|^2 + \frac{\mu}{2} \left(\sin(\alpha)u' - 4 \sin^2\left(\frac{\alpha}{2}\right) \right)^2 + \frac{\mu_c}{2} (\cos(\alpha)u' - 2 \sin(\alpha))^2$$

such that $W_{\alpha\alpha'}(u', \alpha, \alpha') = W_{\alpha'\alpha'}(u', \alpha, \alpha') = 0$. So the second variation (58) w.r.t. α simplifies to

$$D_\alpha^2 E(u, \alpha)(\delta\alpha, \delta\alpha) = \int_0^1 W_{\alpha\alpha}(u', \alpha) \delta\alpha(x)^2 dx. \quad (59)$$

Here and below, we simply write $W(u', \alpha)$ instead of $W(u', \alpha, \alpha')$ due to $L_c = 0$.

Direct computations reveal

$$\begin{aligned} W_\alpha(u', \alpha) &= \mu(\sin(\alpha)u' - 4 \sin^2\left(\frac{\alpha}{2}\right))(\cos(\alpha)u' - 2 \sin(\alpha)) \\ &\quad - \mu_c(\cos(\alpha)u' - 2 \sin(\alpha))(\sin(\alpha)u' + 2 \cos(\alpha)), \\ W_{\alpha\alpha}(u', \alpha) &= (\mu - \mu_c)(\cos(\alpha)u' - 2 \sin(\alpha))^2 + \mu_c(\sin(\alpha)u' + 2 \cos(\alpha))^2 \\ &\quad - \mu(\sin(\alpha)u' - 4 \sin^2\left(\frac{\alpha}{2}\right))(\sin(\alpha)u' + 2 \cos(\alpha)). \end{aligned} \quad (60)$$

- i. For $\mu = \mu_c$, by direct investigation of Equations (44) and (45), we can verify that (\bar{u}, α_2) solves the Euler–Lagrange equations. With Equation (60), we find

$$\begin{aligned} W_{\alpha\alpha}(\bar{u}', \alpha_2) &= \mu(\sin(\alpha_2)\gamma + 2 \cos(\alpha_2))^2 - \mu \left(\sin(\alpha_2)\gamma - 4 \sin^2\left(\frac{\alpha_2}{2}\right) \right) (\sin(\alpha_2)\gamma + 2 \cos(\alpha_2)) \\ &= \mu(\sin(\alpha_2)\gamma + 2 \cos(\alpha_2)) \left(\sin(\alpha_2)\gamma + 2 \cos(\alpha_2) - \underbrace{\sin(\alpha_2)\gamma + 4 \sin^2\left(\frac{\alpha_2}{2}\right)}_{= 2 - 2 \cos(\alpha_2)} \right) \\ &= 2\mu(\sin(\alpha_2)\gamma + 2 \cos(\alpha_2)) \\ &= (\gamma^2 + 4)\mu \cos(\alpha_2). \end{aligned} \quad (61)$$

Next, we observe the identities

$$\cos(\arctan(t)) = \frac{1}{\sqrt{t^2 + 1}}, \quad t \in \mathbb{R}, \quad (62)$$

$$\sin(\arctan(t)) = \frac{t}{\sqrt{t^2 + 1}}, \quad t \in \mathbb{R}. \quad (63)$$

Consequently,

$$\cos(\alpha_2) = \cos\left(\arctan\left(\frac{\gamma}{2}\right)\right) = \frac{2}{(\gamma^2 + 4)^{1/2}}, \quad (64)$$

$$\sin(\alpha_2) = \sin\left(\arctan\left(\frac{\gamma}{2}\right)\right) = \frac{\gamma}{(\gamma^2 + 4)^{1/2}} \quad (65)$$

such that

$$W_{\alpha\alpha}(\bar{u}', \alpha_2) = (\gamma^2 + 4)\mu \cos(\alpha_2) = 2\mu\sqrt{\gamma^2 + 4}.$$

With Equation (59), this implies the strict positivity of the second variation w.r.t. α , that is, there is a constant $K > 0$ such that

$$D_{\alpha}^2 E(\bar{u}, \alpha_2)(\delta\alpha, \delta\alpha) \geq K \|\delta\alpha\|^2 \quad (66)$$

for any test function $\delta\alpha$, proving that (\bar{u}, α_2) is indeed a local minimizer of E , see, for example, Giaquinta and Hildebrandt [25].

ii. For $\mu_c = 0$, the Euler–Lagrange equations read

$$\left[1 - \frac{\cos^2(\alpha)}{2}\right]u'' = [\cos(\alpha) - \sin(\alpha)\cos(\alpha)u' + \sin^2(\alpha) - \cos^2(\alpha)]\alpha', \quad (67)$$

$$0 = (\cos(\alpha)u' - 2\sin(\alpha))\left(\sin(\alpha)u' - 4\sin^2\left(\frac{\alpha}{2}\right)\right). \quad (68)$$

Direct investigation of Equations (67) and (68) shows that (\bar{u}, α_1) , (\bar{u}, α_2) , and (\bar{u}, α_3) are solutions of the Euler–Lagrange equations. With Equation (60), we find

$$\begin{aligned} W_{\alpha\alpha}(\bar{u}', \alpha_1) &= \mu\gamma^2 > 0, \\ W_{\alpha\alpha}(\bar{u}', \alpha_3) &= \mu(\cos(\alpha_3)\gamma - 2\sin(\alpha_3))^2. \end{aligned}$$

Hence, $W_{\alpha\alpha}(\bar{u}', \alpha_3) = 0$ only if $\cos(\alpha_3)\gamma = 2\sin(\alpha_3)$ or equivalently $\alpha_3 := \eta^{-1}(\gamma) = \arctan\left(\frac{\gamma}{2}\right)$, that is, only if $\gamma = \eta(\arctan(\gamma/2))$, that is, only if

$$\gamma = \frac{4\sin^2\left(\frac{\arctan(\gamma/2)}{2}\right)}{\sin(\arctan(\gamma/2))} = \frac{2 - 2\cos(\arctan(\gamma/2))}{\sin(\arctan(\gamma/2))} \quad (69)$$

where Equation (21) was used. With Equations (62) and (63), Equation (69) becomes

$$\gamma = \frac{2 - \frac{2}{\sqrt{1 + \gamma^2/4}}}{\frac{\gamma/2}{\sqrt{1 + \gamma^2/4}}} = \frac{2\sqrt{1 + \frac{\gamma^2}{4}} - 2}{\gamma/2} \Leftrightarrow \gamma^2 = 4\sqrt{1 + \frac{\gamma^2}{4}} - 4 \Leftrightarrow \gamma^2 + 4 = 2\sqrt{4 + \gamma^2}.$$

The last equality is only satisfied for $\gamma = 0$, proving $W_{\alpha\alpha}(\bar{u}', \alpha_3) > 0$ for $\gamma \neq 0$ which yields as in (i) the strict positivity (66) of the second variation w.r.t. α such that (\bar{u}, α_1) and (\bar{u}, α_3) are local minimizers of E .

iii. For $\mu > 0$, $\mu_c > 0$, $\mu \neq \mu_c$, Lemma 3, Case 1 in (ii) shows that (\bar{u}, α_2) solves the Euler–Lagrange Equations (30) and (31).

To verify that (\bar{u}, α_2) is a local minimizer of E , we once more investigate the second variation (59) of E w.r.t. α . Starting from Equation (60), we find

$$\begin{aligned}
 W_{\alpha\alpha}(\bar{u}', \alpha_2) &= (\mu - \mu_c) \underbrace{\left(\cos(\alpha_2)\gamma - 2 \sin(\alpha_2) \right)^2}_{=0} + \mu_c (\sin(\alpha_2)\gamma + 2 \cos(\alpha_2))^2 \\
 &\quad - \mu \left(\sin(\alpha_2)\gamma - 4 \sin^2\left(\frac{\alpha_2}{2}\right) \right) \underbrace{(\sin(\alpha_2)\gamma + 2 \cos(\alpha_2))}_{=2 \cos(\alpha_2) - 2} \\
 &= (\mu_c - \mu) (\sin(\alpha_2)\gamma + 2 \cos(\alpha_2))^2 + 2\mu \underbrace{\left(\sin(\alpha_2)\gamma + 2 \cos(\alpha_2) \right)}_{= \frac{\gamma^2 + 4}{2} \cos(\alpha_2)} \\
 &= \frac{\gamma^2 + 4}{2} \cos(\alpha_2) [2\mu + (\mu_c - \mu) (\sin(\alpha_2)\gamma + 2 \cos(\alpha_2))].
 \end{aligned} \tag{70}$$

Using the formulas (64) and (65) in (70), this yields

$$\begin{aligned}
 W_{\alpha\alpha}(\bar{u}', \alpha_2) &= \frac{\gamma^2 + 4}{2} \frac{2}{\sqrt{\gamma^2 + 4}} \left[2\mu + (\mu_c - \mu) \left(\frac{\gamma^2}{\sqrt{\gamma^2 + 4}} + \frac{4}{\sqrt{\gamma^2 + 4}} \right) \right] \\
 &= \sqrt{\gamma^2 + 4} [2\mu + (\mu_c - \mu) \sqrt{\gamma^2 + 4}].
 \end{aligned}$$

This shows the strict positivity (66) of $D_{\alpha}^2 E(\bar{u}, \alpha_2)(\delta\alpha, \delta\alpha)$, provided the condition (57) holds. \square

Remark 3. We point out that the solution (\bar{u}, α_4) of the Euler–Lagrange equations found in Lemma 3, (ii) is not an independent case. The solution (\bar{u}, α_4) requires $|\frac{\mu - \mu_c}{\mu}| \leq 1$, cf. Equation (53), and then, by the very definition of Case 2 in Lemma 3,

$$\begin{aligned}
 \sin(\alpha_4)\gamma &= 4 \sin^2\left(\frac{\alpha_4}{2}\right) + \frac{2\mu_c}{\mu - \mu_c} = 2 - 2 \cos(\alpha_4) + \frac{2\mu_c}{\mu - \mu_c} \\
 &= 2 - \frac{2(\mu - \mu_c)}{\mu} + \frac{2\mu_c}{\mu - \mu_c} = \frac{2\mu_c}{\mu} + \frac{2\mu_c}{\mu - \mu_c} = \frac{2\mu_c(2\mu - \mu_c)}{\mu(\mu - \mu_c)}.
 \end{aligned} \tag{71}$$

Due to the relationship

$$\sin(\arccos(t)) = \sqrt{1 - t^2} \quad \text{for } t \in [-1, +1], \tag{72}$$

this yields

$$\sin(\alpha_4) = \sqrt{1 - \frac{(\mu - \mu_c)^2}{\mu^2}} = \frac{1}{\mu} \sqrt{\mu_c(2\mu - \mu_c)}. \tag{73}$$

With Equation (71), we obtain

$$\gamma = \frac{2\mu_c(2\mu - \mu_c)}{\mu(\mu - \mu_c) \sin(\alpha_4)} = \frac{2\mu_c(2\mu - \mu_c)}{\mu(\mu - \mu_c)} \frac{\mu}{\sqrt{\mu_c(2\mu - \mu_c)}} = \frac{2\sqrt{\mu_c(2\mu - \mu_c)}}{\mu - \mu_c}. \tag{74}$$

For γ given by Equation (74), we have

$$\begin{aligned} \gamma \cos(\alpha_4) - 2 \sin(\alpha_4) &= \gamma \frac{\mu - \mu_c}{\mu} - \frac{2}{\mu} \sqrt{\mu_c(2\mu - \mu_c)} \\ &= \frac{2\sqrt{\mu_c(2\mu - \mu_c)}}{\mu - \mu_c} \frac{\mu - \mu_c}{\mu} - \frac{2}{\mu} \sqrt{\mu_c(2\mu - \mu_c)} = 0, \end{aligned}$$

leading to $\gamma \cos(\alpha_4) = 2 \sin(\alpha_4)$ or equivalently $(\frac{\gamma}{2}) = \tan(\alpha_4)$. This shows

$$\alpha_4 = \arctan\left(\frac{\gamma}{2}\right) = \alpha_2 \tag{75}$$

for γ given by Equation (74).

To have $\gamma > 0$ in Equation (74), it must hold $0 < \mu_c < \mu$, and the condition $|\frac{(\mu - \mu_c)}{\mu}| \leq 1$ is automatically satisfied.

Remark 4. The following table lists the mechanical energies corresponding to the local minimizers of Corollary 1.

$$(i) \ \mu = \mu_c : \quad E(\bar{u}, \alpha_2) = \mu \left[\gamma^2 + 4 - 2\sqrt{\gamma^2 + 4} \right]. \tag{76}$$

$$(ii) \ \mu_c = 0 : \quad E(\bar{u}, \alpha_1) = E(\bar{u}, \alpha_3) = \frac{\mu}{2} \gamma^2. \tag{77}$$

$$(iii) \ \mu_c > 0, \ \mu \neq \mu_c : \quad E(\bar{u}, \alpha_2) = \mu \left[\gamma^2 + 4 - 2\sqrt{\gamma^2 + 4} \right] \text{ if } \quad 2\mu + (\mu_c - \mu)\sqrt{\gamma^2 + 4} > 0. \tag{78}$$

Remarkably, in all cases, the minimal energy level is independent of the Cosserat couple modulus μ_c .

Remark 5. We want to investigate whether (\bar{u}, α_2) is a minimizer of E in the situation of Remark 3, that is, if

$$0 < \mu_c < \mu \text{ and } (\mu - \mu_c)\gamma = 2\sqrt{\mu_c(2\mu - \mu_c)}. \tag{79}$$

As $\bar{u}'(x) \equiv \gamma$ and assuming that $\alpha(x) \equiv a$ for constant $a \in \mathbb{R}$ and $x \in (0, 1)$, it is enough to investigate the real function

$$f(a) := W(\bar{u}, a) = \frac{\mu}{2} \gamma^2 + \frac{\mu}{2} \left(\gamma \sin(a) - 4 \sin^2\left(\frac{a}{2}\right) \right)^2 + \frac{\mu_c}{2} (\gamma \cos(a) - 2 \sin(a))^2,$$

cf. the definition of W in Equation (19). Straightforward computations yield

$$\begin{aligned} f'(a) &= (\gamma \cos(a) - 2 \sin(a))[(\mu - \mu_c)(\gamma \sin(a) + 2 \cos(a)) - 2\mu], \\ f''(a) &= (\mu - \mu_c) \left[(\gamma \cos(a) - 2 \sin(a))^2 - (\gamma \sin(a) + 2 \cos(a))^2 \right] + 2\mu(\gamma \sin(a) + 2 \cos(a)), \\ f'''(a) &= (\gamma \cos(a) - 2 \sin(a))[2\mu - 4(\mu - \mu_c)(\gamma \sin(a) + 2 \cos(a))], \\ f^{(4)}(a) &= 4(\mu - \mu_c) \left[(\gamma \sin(a) + 2 \cos(a))^2 - (\gamma \cos(a) - 2 \sin(a))^2 \right] - 2\mu(\gamma \sin(a) + 2 \cos(a)). \end{aligned}$$

Remarkably, $f'(\alpha_2) = f''(\alpha_2) = f'''(\alpha_2) = 0$, but

$$f^{(4)}(\alpha_2) = \frac{12\mu^2}{\mu - \mu_c} > 0,$$

showing that α_2 is a minimizer of f and indicating that (\bar{u}, α_2) is a local minimizer of E for constant $\alpha(x) \equiv \alpha_2$ under the choice of parameters (79). The minimal energy coincides with Equation (78) for γ

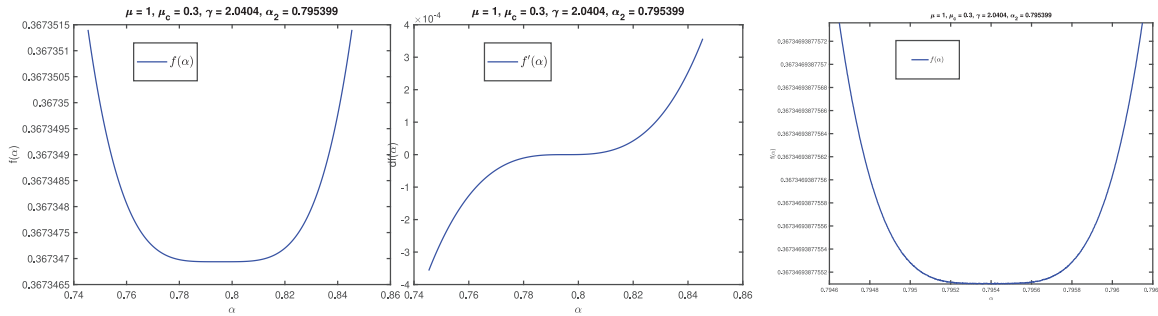


Figure 6. Left and center: Plot of $f(\alpha)$, $f'(\alpha)$ near α_2 for $\mu = 1$, $\mu_c = 0.3$ and γ given by Equation (74). Right: Close-up of $f(\alpha)$ near α_2 . The tiny oscillations of the graph near α_2 in the close-up are numerical rendering artifacts generated by MATLAB.

given by Equation (74). Due to $f'(\alpha_2) = f''(\alpha_2) = f'''(\alpha_2) = 0$, the function f is extremely flat near α_2 , making it very difficult to numerically compute the correct minimizer (see Figure 6).

Remark 6. Let $\mu > 0$ and $\gamma > 0$ be given. Then in the limit $\mu_c \searrow 0$, Equation (57) is not satisfied, as Equation (57) for $\mu_c = 0$ leads to the contradiction

$$2 - \sqrt{\gamma^2 + 4} > 0.$$

So, for small $\mu_c > 0$, the necessary Legendre condition $D_\alpha^2 E(\bar{u}, \alpha_2)(\delta\alpha, \delta\alpha) \geq 0$ is violated and (\bar{u}, α_2) is no local minimizer of E , especially in Corollary 1, (ii). Contrary, for $\mu_c > 0$ large enough, (57) clearly holds. In conclusion, for

$$\mu_c > \mu_c^{\text{crit}} := \mu \left[1 - \frac{2}{\sqrt{\gamma^2 + 4}} \right], \tag{80}$$

Equation (57) is valid and (\bar{u}, α_2) is a minimizer of E . This result is also confirmed by our numerical simulations (cf. Figure 12).

Remark 7. It is instructive to compare Corollary 1 and Remark 4 with the results in Fischle and Neff [26], stating that

$$\text{For } \mu_c \geq \mu > 0 : \quad W_{\mu, \mu_c}(R; F) \sim W_{1,1}(R; F), \tag{81}$$

$$\text{For } \mu > \mu_c \geq 0 : \quad W_{\mu, \mu_c}(R; F) \sim W_{1,0}(R; \tilde{F}_{\mu, \mu_c}). \tag{82}$$

Here, $F = D\varphi \in \mathbb{R}^{n \times n}$ is a given deformation gradient, $\tilde{F}_{\mu, \mu_c} := ((\mu - \mu_c)/\mu)F$,

$$f \sim g : \Leftrightarrow \operatorname{argmin}_{R \in \text{SO}(n)} f(R) = \operatorname{argmin}_{R \in \text{SO}(n)} g(R)$$

for two functions f and g , and

$$W_{\mu, \mu_c}(R; F) := \mu |\operatorname{sym}(R^T F - \mathbb{1}_3)|^2 + \mu_c |\operatorname{skew}(R^T F - \mathbb{1}_3)|^2 \tag{83}$$

which coincides with Equation (19) for $L_c = 0$, F given by Equation (12), and $R \in \text{SO}(3)$ defined by Equation (13).

Replacing $W_{\mu, \mu_c}(R; F)$ by $W_{1,0}(R; \tilde{F}_{\mu, \mu_c})$ corresponds to rescaling the parameters of E in Equation (19) by

$$\tilde{\mu} := \frac{(\mu - \mu_c)^2}{\mu^2}, \quad \tilde{\mu}_c := 0$$

while leaving γ unchanged. Indeed this rescaling does not affect neither the constant minimizer α_1 nor α_2 and α_3 which are independent of μ, μ_c and are functions of γ , only. In conclusion, Corollary 1 and Remark 4 confirm the results in Fischle and Neff [26].

4. Numerical simulations for vanishing internal length scale

For $L_c > 0$, various advanced numerical tools such as multigrid methods are available [27]. We will not discuss this here. In contrast, the case $L_c = 0$ is numerically challenging as the regularizing term $2\mu L_c^2 |\alpha'|^2$ in E and E_{red} disappears in the limit. We investigate the problem in two different ways and compare the solution strategies. We begin with the situation of non-regular solutions with $\alpha \in L^4(\Omega)$.

1. Newton-GMRES algorithm

For $L_c = \mu_c = 0$ and $\alpha \in L^4(\Omega)$, the solutions (u, α) to $E_{\text{red}}(u, \alpha) \rightarrow \min$ satisfy pointwise for $x \in \Omega = (0, 1)$ the two purely algebraic equations (see Neff and Münch [20, Equation (3.30)] for a derivation),

$$\alpha(\alpha - u') \left(\alpha - \frac{u'}{2} \right) = 0, \tag{84}$$

$$(u' - \zeta) \left(u' + \frac{1}{8} (u')^3 - \zeta \right) = 0 \tag{85}$$

subject to the boundary conditions

$$u(0) = 0, \quad u(1) = \gamma, \quad u'(0) = u'(1), \quad \alpha(0) = \alpha(1) = \alpha_D \tag{86}$$

for a constant $\alpha_D \in \mathbb{R}$ and with $\zeta := (1 + \alpha_D^2)u'(0) - \alpha_D^3$. In general, there is a multitude of solutions to (84)–(86). To specify a solution, one may prescribe a volume fraction $\theta \in [0, 1]$ such that

$$\mathcal{L}^1(\{x \in \Omega \mid \alpha(x) = 0\}) = \theta, \tag{87}$$

where \mathcal{L}^1 denotes the one-dimensional Lebesgue measure. To compute solutions to Equations (84)–(86), the derivative u' is approximated by central difference quotients leading to a discrete problem in the standard form

$$\text{Find } x \in \mathbb{R}^{2N-3} : \quad G(x) = 0 \tag{88}$$

for a differentiable function $G : \mathbb{R}^{2N-3} \mapsto \mathbb{R}^{2N-3}$ and with $N \in \mathbb{N}$ denoting the number of discretization points in Ω . The solutions to Equation (88) are computed using a Newton-GMRES method where the Fréchet derivative DG of G is approximated by

$$DG(x)d \sim \frac{G(x + \delta d) - G(x)}{\delta} \tag{89}$$

for suitable small $\delta > 0$ and GMRES is used to solve the linearized equations. While the algorithm computes DG automatically thanks to Equation (89), its practicability is limited by the huge memory requirements. The implementation details related to the definition of G are left out here.

2. BFGS Quasi-Newton method

As in the first method, the values of α , α' , and u' are discretized along $N \in \mathbb{N}$ points $z_i \in \Omega$. Letting $f_i := W(u'(z_i), \alpha(z_i), \alpha'(z_i))$ be the integrand either in (18) or in (24), the repeated Trapezoidal rule

$$\left(\frac{1}{2}f_1 + \sum_{i=2}^{N-1} f_i + \frac{1}{2}f_N \right)$$

is used for the approximate integration. The minimization of the functional is carried out by a Quasi-Newton method where the approximate Hessian is computed by the Broyden-Fletcher-Goldfarb-Shanno update formula [28]. Again, we leave out the implementation details, but refer to Blesgen [29–31], where the limited-memory variant of the algorithm is applied to Cosserat plasticity and recrystallization.

In comparison, both algorithms compute the same solutions. However, the BFGS Quasi-Newton method is capable of handling larger values of N due to the tremendous memory needs of the Newton-GMRES scheme.

Figure 7 displays three minimizers of E_{red} in \mathcal{X}^D for different values of N and prescribed slope $u'(0)$ at the boundary. The deformation u_N forms a sawtooth pattern with alternating, constant slopes, while the values of randomly concentrate at 0 and γ . The computations of Figure 7 suggest further that u_N converges to the homogeneous deformation $\bar{u}(x) := \gamma x$ as $N \rightarrow \infty$.

Figures 8 and 9 compare the minimizers of E_{red} in \mathcal{X}^C and \mathcal{X}^D for three different values of N . Again, α randomly concentrates at 0 and γ while the deformation u_N forms a sawtooth pattern with alternating, constant slopes. The computed deformation u is extremely close to \bar{u} but energetically beats the homogeneous solution.

We will adopt the following notation in the set $\mathcal{M}^+(\mathbb{R})$ of finite positive Radon measures. For a sequence $(\nu_j)_{j \in \mathbb{N}}$ and a Carathéodory function f such that

$$f(x, \nu_j) \rightharpoonup \left(x \mapsto \int_{\mathbb{R}} f(x, A) d\nu_x(A) \right) \quad \text{in } L^1(\mathbb{R})$$

for a parameterized measure $\nu = (\nu_x)_{x \in \mathbb{R}}$, we use the shorthand notation $\nu_j \xrightarrow{Y} \nu$.

Remark 8. The numerical computations in Figures 7–9 indicate the following result regarding non-regular solutions.

Let $L_c = 0$ and $(u_N, \alpha_N)_{N \in \mathbb{N}}$ be a minimizing sequence of E_{red} in $W^{1,2}(\Omega) \times L^4(\Omega)$ with $u_N(x) \rightharpoonup \bar{u}(x)$, $\alpha_N \rightharpoonup \alpha$ for $N \rightarrow \infty$. Then, there is a (not relabelled) subsequence and a constant $\theta \in [0, 1]$ such that

$$W_{\text{red}}(u_N, \alpha_N) \xrightarrow{Y} \theta \delta_0 + (1 - \theta) \delta_\gamma. \tag{90}$$

The existence of a limiting Young measure generated by the subsequence (u_N, α_N) can be made rigorous by applying the fundamental theorem of Young measures, see, for example, Müller [32]. We observe that the family $(W_{\text{red}}(u_N, \alpha_N))_{N \in \mathbb{N}}$ is uniformly bounded in L^1 and equi-integrable by the Dunford-Pettis theorem.

Figure 10 displays minimizers of E in \mathcal{X}^C . Except near $\partial\Omega = \{0, 1\}$, the minimizing rotation α takes constant values with either $\alpha \equiv \alpha_1 := 0$ or $\alpha \equiv \alpha_3 := \eta^{-1}(\gamma)$ in accordance with Corollary 1 (ii). Depending on the initial values at start of the optimization, the BFGS-algorithm computes one of two different minimizers u which both converge in Ω to $\bar{u}(x)$ as $N \rightarrow \infty$. The first, u_1 with $\alpha \equiv \alpha_1$, is a straight line except near $\partial\Omega$. The second, u_2 with $\alpha \equiv \alpha_3$, leads to a scaled function

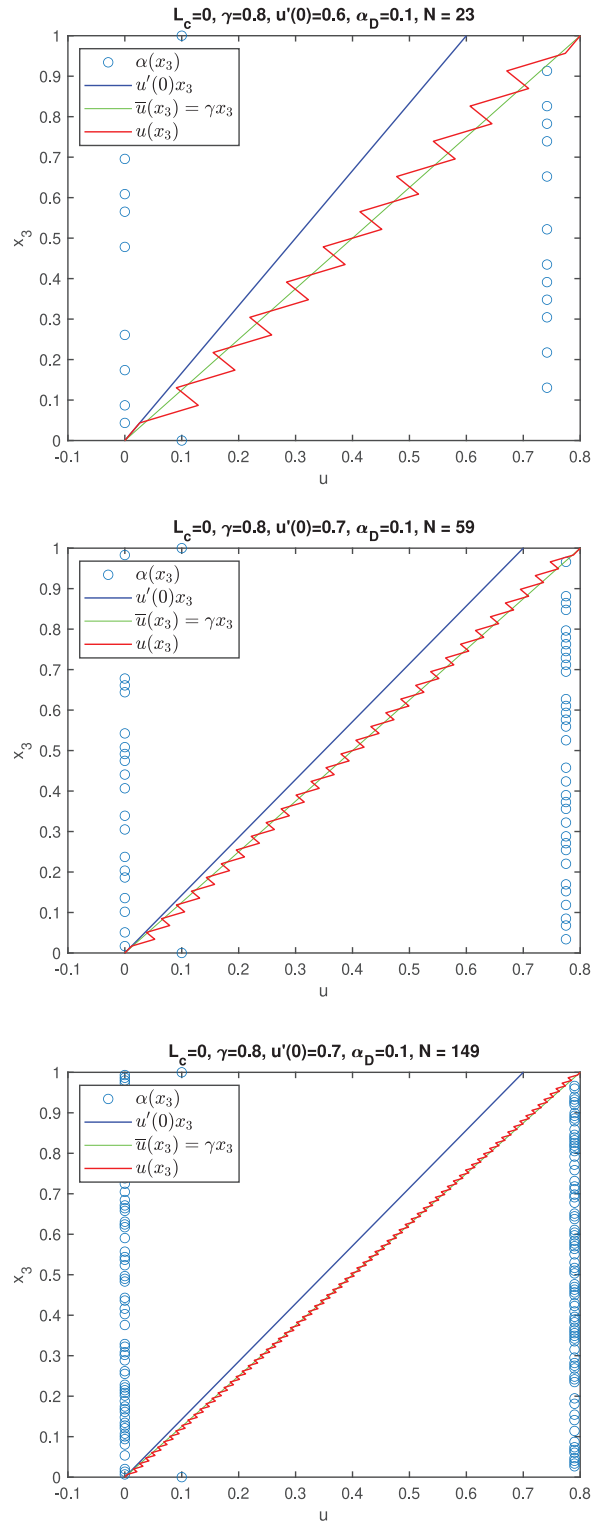


Figure 7. Minimizers of E_{red} in \mathcal{X}^c for $N = 23$, $N = 59$, and $N = 149$ for $\mu = 1$, $\mu_c = 0$, $\gamma = 0.8$, prescribed $u'(0) = u'(1)$ (blue line) and $\alpha_D = u(0) = u(1) = 0.1$. The blue balls are the computed values of α randomly concentrating at 0 and γ . The green line displays the homogeneous deformation $\bar{u}(x) = \gamma x$. The deformation u is rendered in red forming a microstructure with a sawtooth pattern.

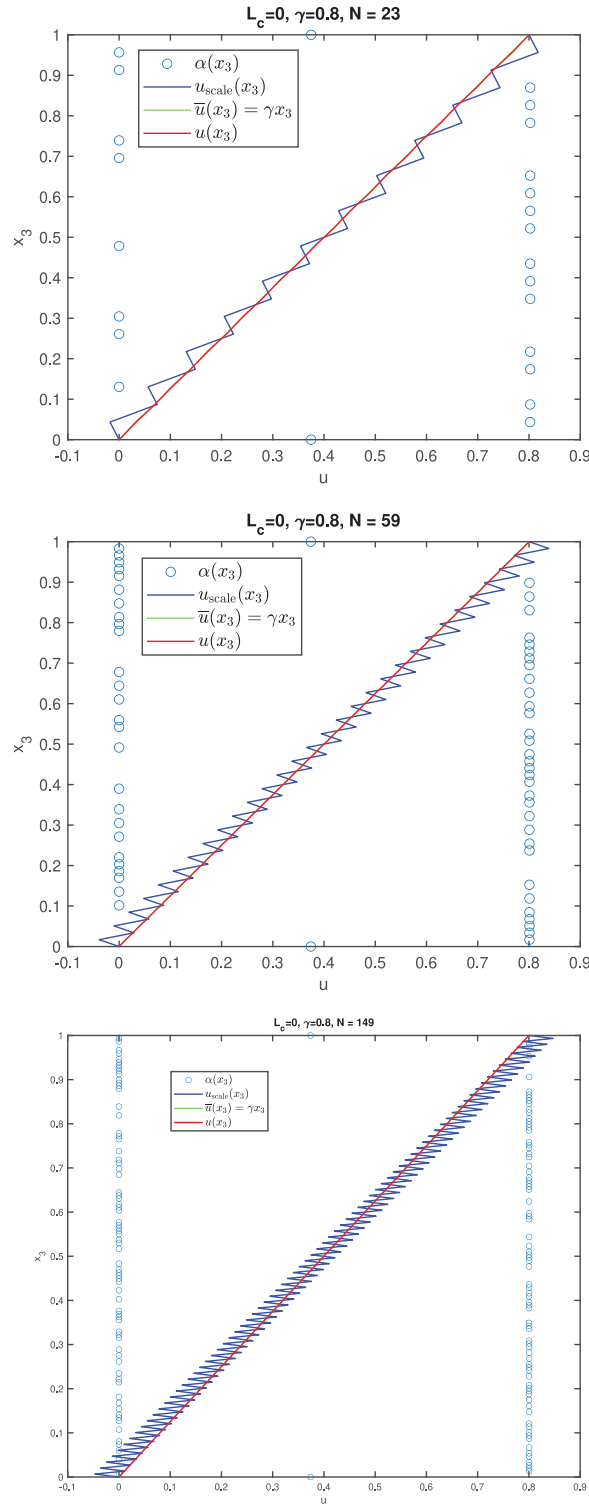


Figure 8. Minimizers of E_{red} in \mathcal{X}_{red}^C for $N = 23, N = 59$, and $N = 149$ for $\mu = 1, \mu_c = 0, \gamma = 0.8$. The blue balls are the computed values of α randomly concentrating at 0 and γ . The deformation u is rendered in red and forms a microstructure with a sawtooth pattern which is extremely close to the homogeneous deformation $\bar{u}(x) = \gamma x$ rendered in green. The differences between u and \bar{u} are amplified by the blue line rendering the rescaled deformation $u_{scale}(x) := \gamma x + N(u(x) - \gamma x)$. The value $\alpha(0)$ is strictly smaller than $\gamma/2$ and indicates by which amount the sawtooth solution u energetically beats the homogeneous solution.

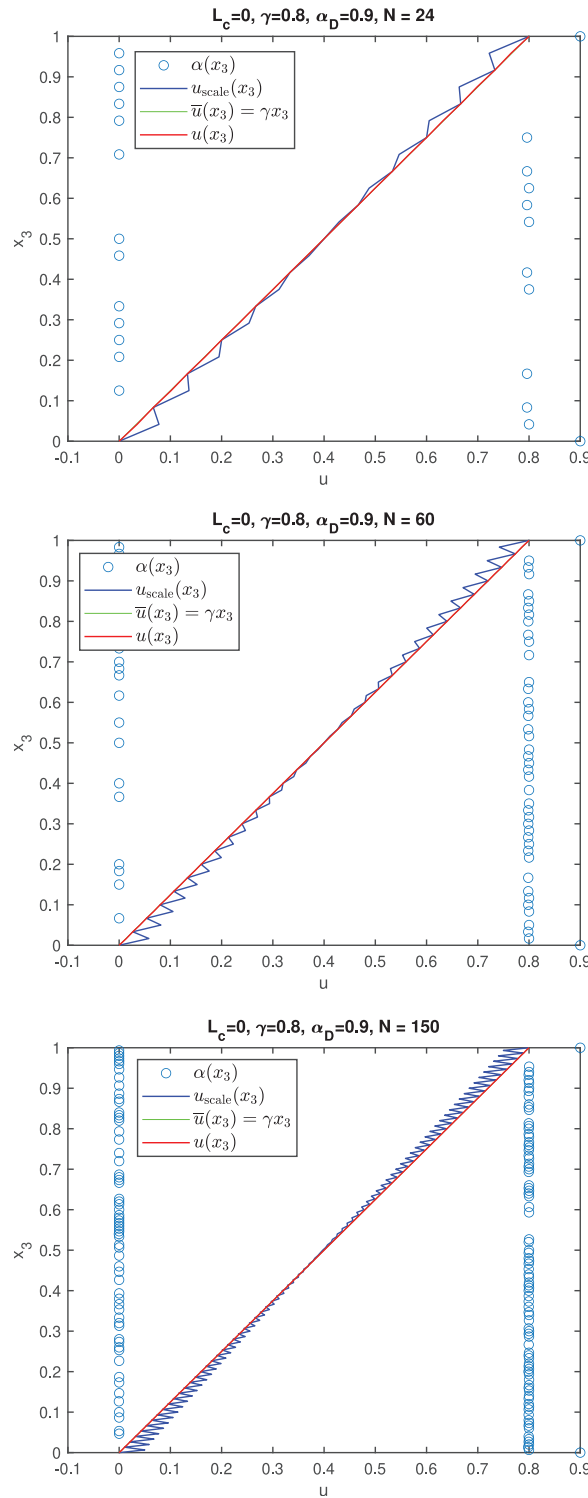


Figure 9. Minimizers of E_{red} in λ^D for $N = 24$, $N = 60$, and $N = 150$ for $\mu = 1$, $\mu_c = 0$, $\gamma = 0.8$. The blue balls are the computed values of α randomly concentrating at 0 and γ . The deformation u is rendered in red and forms a microstructure with a sawtooth pattern which is extremely close to the homogeneous deformation $\bar{u}(x) = \gamma x$ rendered in green. The blue line is the rescaled deformation $u_{\text{scale}}(x) := \gamma x + N(u(x) - \gamma x)$ amplifying the differences between u and \bar{u} . As can be seen, the oscillation of u is largest near $\partial\Omega$ and smallest at $x = 0.5$.

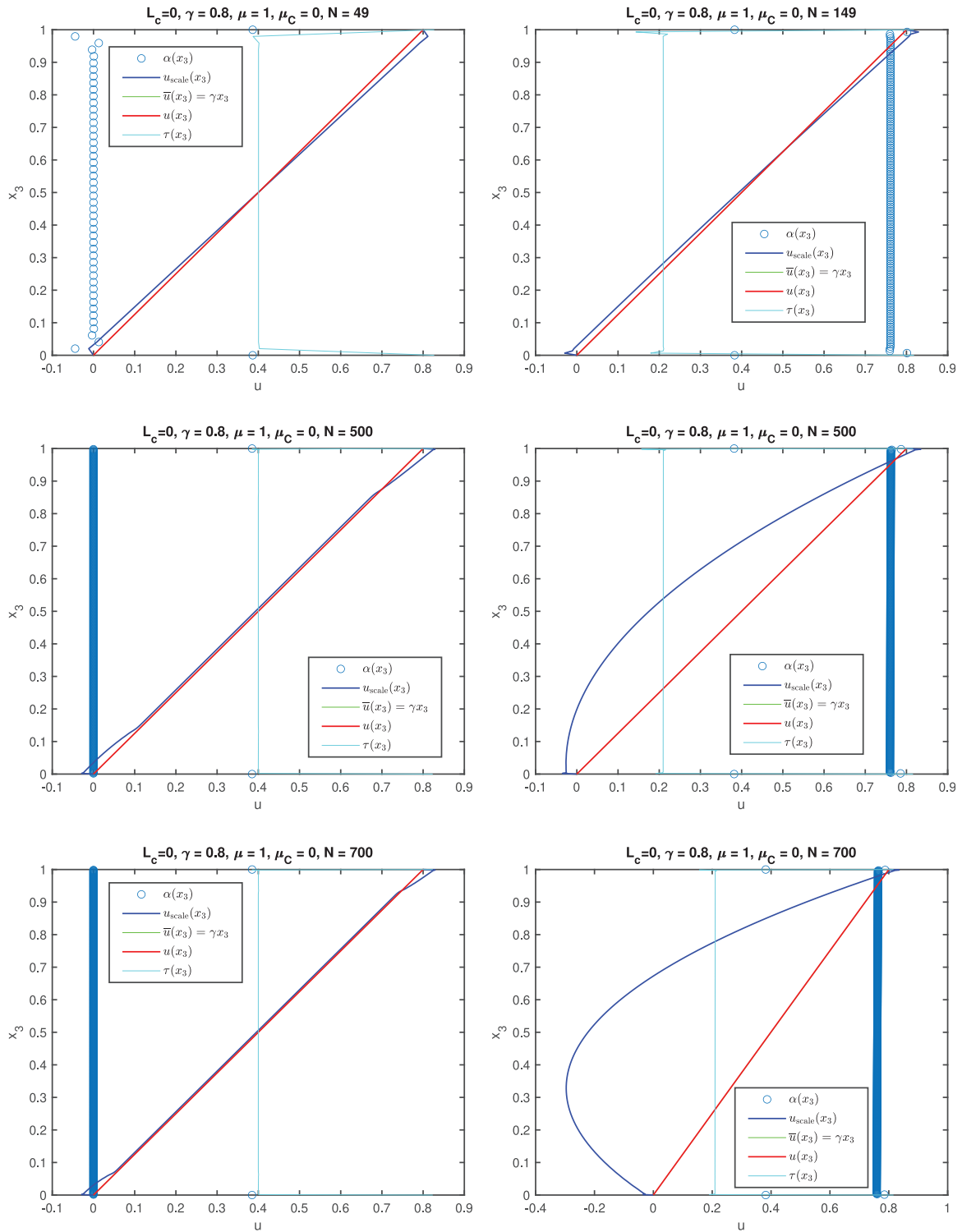


Figure 10. Minimizers of E in \mathcal{X}^C for $\mu = 1, \mu_c = 0, \gamma = 0.8$ and $N = 49, N = 149, N = 500, N = 700$. The blue balls are the computed values of α with either $\alpha \equiv \alpha_1 = 0$ or $\alpha \equiv \alpha_3 = \eta^{-1}(\gamma) = 0.760053$. In cyan the computed stress tensor τ which is constant in Ω . The deformation u is rendered in red, extremely close to $\bar{u}(x) = \gamma x$ rendered in green. The blue line is the rescaled deformation $u_{\text{scale}} := \gamma x + N(u(x) - \gamma x)$.

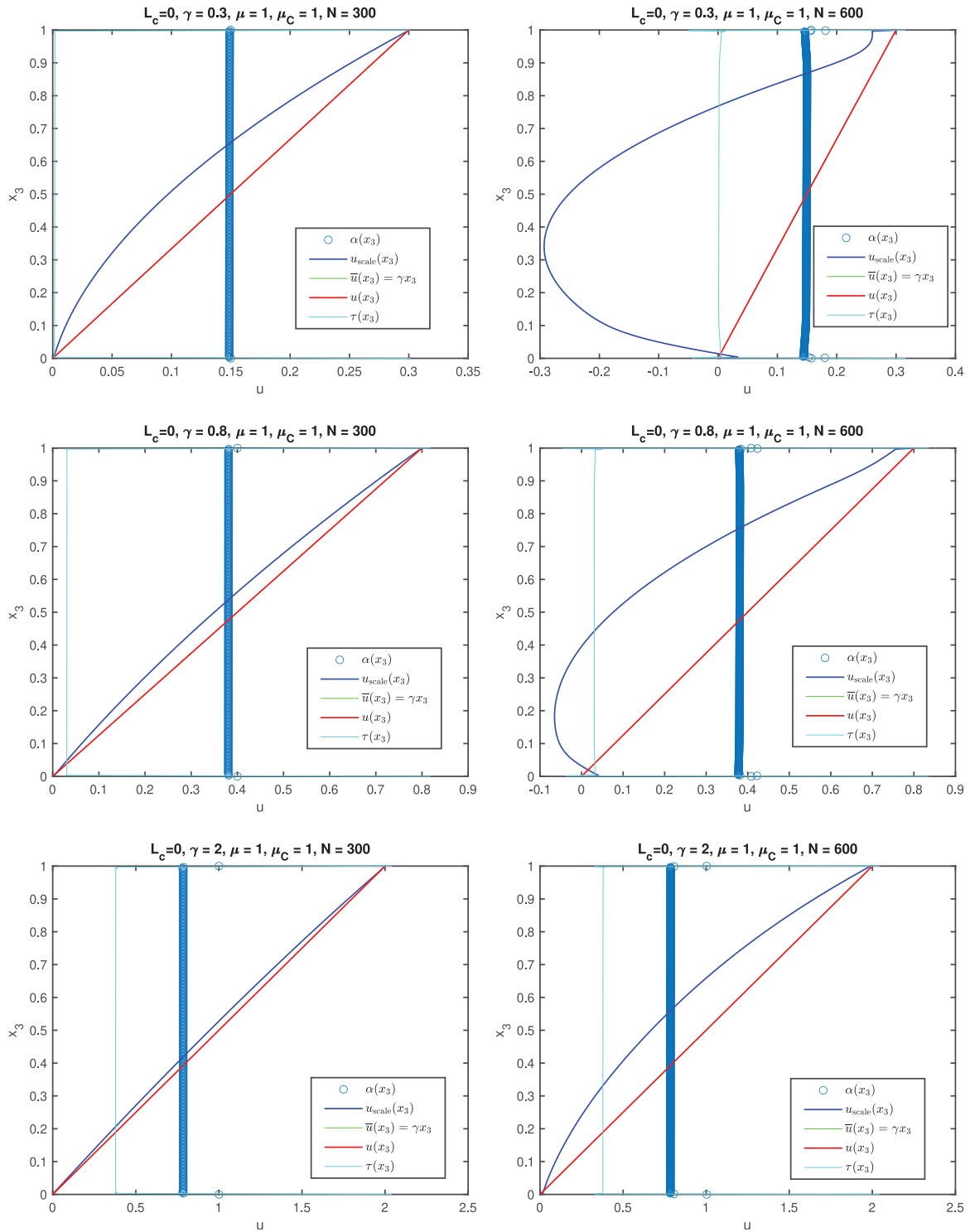


Figure 11. Minimizers of E in \mathcal{X}^C for $\mu = \mu_c = 1$ and $N = 300$ (left), $N = 600$ (right) and $\gamma = 0.3$ top line, $\gamma = 0.8$ center, and $\gamma = 2.0$ bottom line. The blue balls are the computed values of α with either $\alpha \equiv 0.14868 \sim \alpha_2 = \arctan(0.15) = 0.14889$ (top), $\alpha \equiv 0.3804 \sim \alpha_2 = \arctan(0.4) = 0.380506$ (center), and $\alpha \equiv 0.7852 \sim \alpha_2 = \arctan(1) = 0.785398$ (bottom) as predicted by Corollary 1 (i). In cyan the computed stress tensor τ . The deformation u is rendered in red, extremely close to $\bar{u}(x) = \gamma x$ rendered in green. The blue line is the rescaled deformation $u_{\text{scale}} := \gamma x + N(u(x) - \gamma x)$.

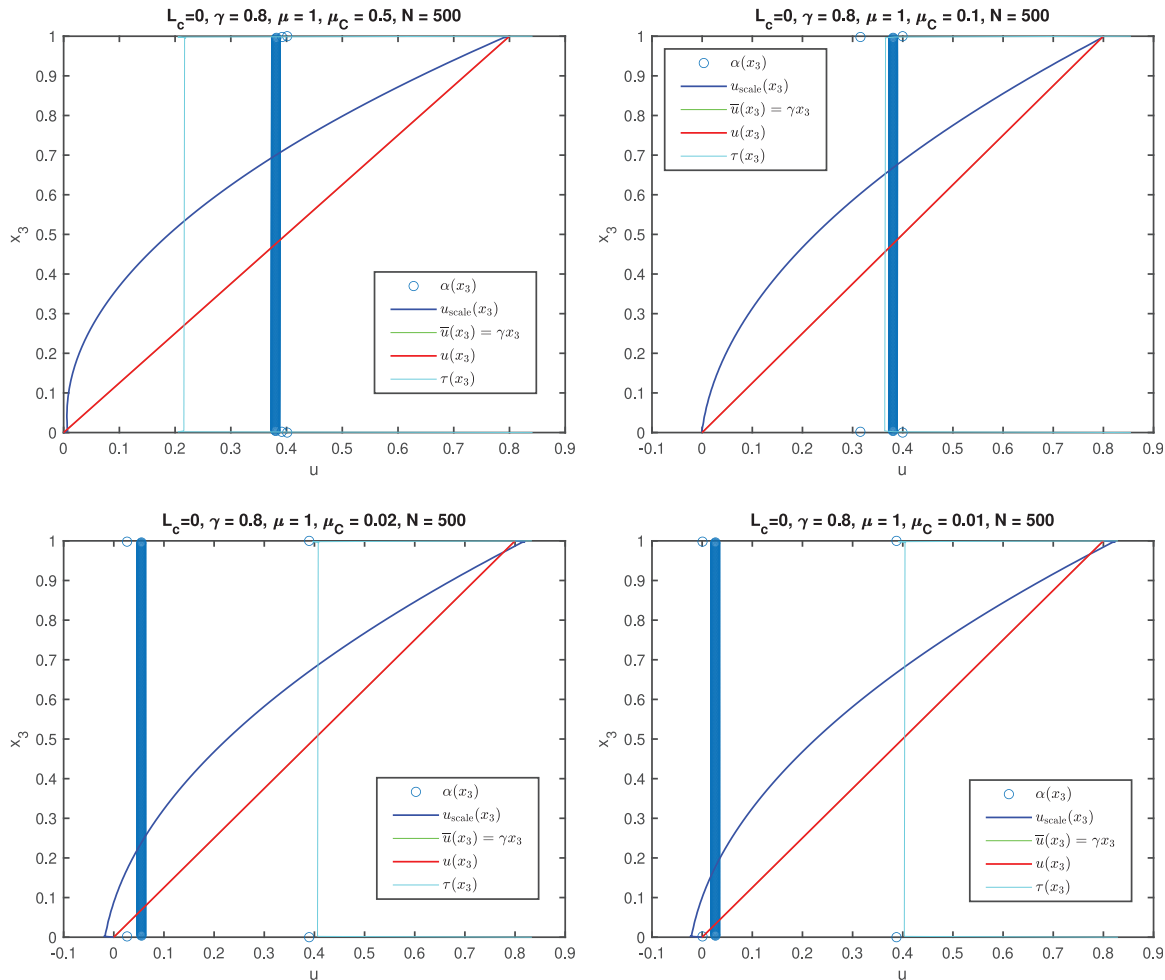


Figure 12. Minimizers of E in \mathcal{X}^C for $\mu = 1$, $\gamma = 0.8$, and $N = 500$. Top left: $\mu_c = 0.5$ with $\alpha \equiv 0.3801 \approx \alpha_2 = \arctan(\gamma/2)$. Top right: $\mu_c = 0.1$ with $\alpha \equiv 0.3804 \approx \alpha_2$. Bottom left: $\mu_c = 0.02$ with $\alpha \equiv 0.0548 \neq \alpha_2$. Bottom right: $\mu_c = 0.01$ with $\alpha \equiv 0.026 \neq \alpha_2$. The results underline the validity of Corollary 1 (iii) and demonstrate that for μ_c small enough, α_2 is no longer a minimizer of E (cf. Remark 6). The critical value of μ_c predicted by (80) is $\mu_c^{\text{crit}} \approx 0.0715$. In cyan the computed stress tensor τ . The deformation u is rendered in red, extremely close to $\bar{u}(x) = \gamma x$ rendered in green. The blue line is the rescaled deformation $u_{\text{scale}} := \gamma x + N(u(x) - \gamma x)$.

$u_{\text{scale}}(x) := \gamma x + N(u_2(x) - \gamma x)$ which is a bended curve (see Figure 10). The energy levels of both computed local minimizers are extremely close with

$$E(u_1, \alpha_1) = 0.32001744, \quad E(u_2, \alpha_3) = 0.320018, \quad (91)$$

confirming Equation (77). Yet, numerical optimization favors (\bar{u}, α_1) over (\bar{u}, α_3) , underlining that the energy landscape for geometrically nonlinear Cosserat materials is extremely complicated and emphasizing why it is so hard to numerically compute the correct global minimizers. In comparison with Equation (91), the theoretical infimal energy is $E(\bar{u}, \alpha_1) = \frac{\mu}{2} \gamma^2 = 0.32$, but (\bar{u}, α_1) violates the consistent coupling condition (27).


Figure 11 studies minimizers in \mathcal{X}^C related to Corollary 1, (i). Again, $u_N \rightarrow \bar{u}$ in Ω for $N \rightarrow \infty$. The minimizing microrotation angle α is constant (except near $\partial\Omega$) and takes the values predicted by Corollary 1.

Figure 12 confirms the validity of Corollary 1, (iii) and of Condition (80). The numerical results indicate that for $\mu_c > 0$ large enough, $\alpha_2 = \arctan(\gamma/2)$ is a local minimizer of $E(\bar{u}, \cdot)$ while for μ_c close to 0, this is no longer true.

Funding

The author(s) received no financial support for the research, authorship, and/or publication of this article.

ORCID iD

Thomas Blesgen  <https://orcid.org/0000-0003-4765-926X>

References

- [1] Capriz, G. *Continua with microstructure*. New York: Springer, 1989.
- [2] Cosserat, E, and Cosserat, F. *Théorie des corps déformables* (Paul Appell). Paris: Gauthier-Villars, 1909.
- [3] Cosserat, E, and Cosserat, F. Note sur la théorie de l'action euclidienne. (Appendix in Appell, 1893: 557–629).
- [4] Appell, P. *Traité de mécanique rationnelle: Statique. Dynamique du point* (Vol. 1). Paris: Gauthier-Villars, 1893.
- [5] Neff, P, Fischle, A, and Münch, I. Symmetric Cauchy stresses do not imply symmetric Biot strains in weak formulations of isotropic hyperelasticity with rotational degrees of freedom. *Acta Mech* 2008; 197(1): 19–30.
- [6] Biršan, M, and Neff, P. On the dislocation density tensor in the Cosserat theory of elastic shells. In: Naumenko, K, and Assmus, M (eds) *Advanced methods of continuum mechanics for materials and structures, advances structures materials*, 60. New York: Springer, 2016, pp. 391–413.
- [7] Neff, P, and Münch, I. Curl bounds Grad on. *ESAIM—Control Optim Calc Var* 2008; 14(1): 148–159.
- [8] Neff, P. Existence of minimizers for a geometrically exact Cosserat solid. *Proc Appl Mathe Mech* 2004; 4(1): 548–549.
- [9] Neff, P, Biršan, M, and Osterbrink, F. Existence theorem for geometrically nonlinear Cosserat micropolar model under uniform convexity requirements. *J Elast* 2015; 121(1): 119–141.
- [10] Lankeit, J, Neff, P, and Osterbrink, F. Integrability conditions between the first and second Cosserat deformation tensor in geometrically nonlinear micropolar models and existence of minimizers. *Z Angew Math Phys* 2017; 68(1): 1–19.
- [11] Mariano, PM, and Modica, G. Ground states in complex bodies. *ESAIM—Control Optim Calc Var* 2009; 15(2): 377–402.
- [12] Li, Y, and Wang, C. Regularity of weak solution of variational problems modeling the Cosserat micropolar elasticity. *Int Math Res Notice* 2022; 2022(6): 4620–4658.
- [13] Gastel, A. Regularity issues for Cosserat continua and p-harmonic maps. *SIAM J Mathe Anal* 2019; 51(6): 4287–4310.
- [14] Neff, P, Lankeit, J, and Madeo, A. On Grioli's minimum property and its relation to Cauchy's polar decomposition. *Int J Eng Sci* 2014; 80: 209–217.
- [15] Fischle, A, Neff, P, and Raabe, D. The relaxed-polar mechanism of locally optimal Cosserat rotations for an idealized nanoindentation and comparison with 3D-EBSD experiments. *Z Angew Math Phys* 2017; 68(4): 1–30.
- [16] Borisov, L, Fischle, A, and Neff, P. Optimality of the relaxed polar factors by a characterization of the set of real square roots of real symmetric matrices. *Z Angew Mathe Mech* 2019; 99(6): e201800120.
- [17] Neff, P, Fischle, A, and Borisov, L. Explicit global minimization of the symmetrized Euclidean distance by a characterization of real matrices with symmetric square. *SIAM J Appl Algebra Geomet* 2019; 3(1): 31–43.
- [18] Birtea, P, Cașu, I, and Comănescu, D. Characterization of the critical points for the shear-stretch strain energy of a Cosserat problem. *Z Angew Math Phys* 2020; 71(2): 1–17.
- [19] Dmitrieva, O, Dondl, PW, Müller, S, et al. Lamination microstructure in shear deformed copper single crystals. *Acta Material* 2009; 57(12): 3439–3449.
- [20] Neff, P, and Münch, I. Simple shear in nonlinear Cosserat elasticity: bifurcation and induced microstructure. *Contin Mech Thermo* 2009; 21(3): 195–221.
- [21] d'Agostino, MV, Rizzi, G, Khan, H, et al. The consistent coupling boundary condition for the classical micromorphic model: existence, uniqueness and interpretation of parameters. arXiv preprint arXiv: 2112.12050, 2021.
- [22] Struwe, M. *Variational methods: applications to nonlinear partial differential equations and Hamiltonian systems*. 4th ed. Berlin: Springer, 2008.
- [23] Dacorogna, B. *Direct methods in the calculus of variations*. 2nd ed. Berlin: Springer, 2008.
- [24] Acerbi, E, and Fusco, N. Semicontinuity problems in the calculus of variations. *Arch Ration Mech Anal* 1984; 86: 125–145.
- [25] Giaquinta, M, and Hildebrandt, S. *Calculus of variations I*. Berlin: Springer, 2004.
- [26] Fischle, A, and Neff, P. The geometrically nonlinear Cosserat micropolar shear-stretch energy. Part I: a general parameter reduction formula and Energy-minimizing Microrotations in 2D. *Z Angew Math Mech* 2017; 97(7): 843–871.
- [27] Blesgen, T, and Amendola, A. Mathematical analysis of a solution method for finite-strain holonomic plasticity of Cosserat materials. *Meccanica* 2020; 55: 621–636.
- [28] Broyden, CG. The convergence of a class of double-rank minimization algorithms. *J Insti Math Appli* 1970; 6: 76–90.
- [29] Blesgen, T. Deformation patterning in Cosserat plasticity. *Model Simul Mat Sci Eng* 2013; 21(3): 35001–35012.
- [30] Blesgen, T. Deformation patterning in three-dimensional large-strain Cosserat plasticity. *Mech Res Commun* 2014; 62: 37–43.

- [31] Blesgen, T. A variational model for dynamic recrystallization based on Cosserat plasticity. *Composites B* 2017; 115: 236–243.
- [32] Müller, S. Variational models for microstructure and phase transitions, Lecture Notes no. 2, Max-Planck-Institute for Mathematics, 1998. <https://www.mis.mpg.de/publications/other-series/ln/lecturenote-0298.html>

DuEPublico

Duisburg-Essen Publications online

UNIVERSITÄT
DUISBURG
ESSEN

Offen im Denken

ub

universitäts
bibliothek

This text is made available via DuEPublico, the institutional repository of the University of Duisburg-Essen. This version may eventually differ from another version distributed by a commercial publisher.

DOI: 10.1177/10812865221122191

URN: urn:nbn:de:hbz:465-20240502-170242-7

This publication is with permission of the rights owner freely accessible due to an Alliance licence and a national licence (funded by the DFG, German Research Foundation) respectively.

© The Author(s) 2022. All rights reserved.

Article reuse guidelines: <https://uk.sagepub.com/en-gb/eur/journals-permissions>